# Grid Integration of Wind Power Systems: Modeling of Wind Power Plants

**Mithun Vyas, Mohit Singh and Surya Santoso**

**Abstract** In the United States, wind power is expected to make up a significant portion of future generation portfolios. A scenario in which wind power will supply 20 % of U.S. peak demand by 2030 has been examined and found feasible [1]. A challenge facing power system planners and operators, in the near future, is the grid integration of large amounts of wind power. To determine the impacts of large wind power plants on system stability, reliable computer models are necessary. However, wind turbine models are not readily available in most dynamic simulation software. The diversity and manufacturer-specific nature of technologies used in commercial wind turbines exacerbates the modeling problem. A solution to this problem is to develop a generic, manufacturer-independent modeling framework that can be implemented in any software capable of simulating power system dynamics.

## 1 Introduction

### *1.1 Motivation*

In the United States, wind power is expected to make up a significant portion of future generation portfolios. A scenario in which wind power will supply 20 % of U.S. peak demand by 2030 has been examined and found feasible [1]. A challenge facing power system planners and operators, in the near future, is the grid integration of large amounts of wind power. To determine the impacts of large wind power plants on system stability, reliable computer models are necessary. However, wind turbine models are not readily available in most dynamic simulation software. The diversity and manufacturer-specific nature of technologies used in commercial wind turbines exacerbates the modeling problem. A solution to this

M. Vyas · M. Singh · S. Santoso (✉)
The University of Texas at Austin, Austin, USA
e-mail: ssantoso@mail.utexas.edu

P. M. Pardalos et al. (eds.), *Handbook of Wind Power Systems*, Energy Systems,
DOI: 10.1007/978-3-642-41080-2_6, 

problem is to develop a generic, manufacturer-independent modeling framework that can be implemented in any software capable of simulating power system dynamics. This chapter describes the development of generic models for:

1. A fixed-speed wind turbine,
2. A wind turbine employing the principle of rotor resistance control, and
3. A turbine with a doubly-fed induction machine employing flux-vector control (DFIG).

The focus of this chapter is on wind turbines which use induction generators, since they comprise the largest installed base of wind turbines and also have more significant effects on the bulk power system than other machines. A detailed description of the wind turbine models is provided along with details of their implementation on two different software platforms, widely used in industry and academia namely PSCAD/EMTDC and MATLAB/SIMULINK. While the central purpose of these models is to study the interaction between the wind turbine and the power system, they may also be used to examine the interaction of aerodynamic, mechanical, and electrical functions within the wind turbine.

## *1.2 Wind Turbine Technologies*

Fixed-speed wind turbines are so named because they operate with less than 2 % variation in turbine rotor speed. They employ squirrel-cage induction machines directly connected to the power grid. The rotor blades are attached to the hub at a fixed pitch, and are designed in such a manner that the air flow over the blades changes from streamline flow to turbulent flow at high wind speeds. This limits the kinetic power extracted from the wind at high wind speeds in order to protect the induction machine and drive train between overheating and overspeeding. Turbines using this design are known as stall-regulated. A side-effect of stall regulation is that energy capture from the wind is sub-optimal. In contrast, variable-speed wind turbines are designed to operate at a wide range of rotor speeds. The rotor speed may vary with the wind speed, or with other system variables, depending on the design employed. Typically in variable-speed turbines, the blades are not rigidly fixed to the hub, and can be rotated a few degrees to turn them out of or into the wind. Additional speed and power controls allow these turbines to extract more energy from a wind regime than would be possible with fixed-speed turbines. For DFIG turbines, power converters are needed to interface the wind turbine and the grid. One important advantage of converter-based systems is that they allow independent real and reactive power control.

Fixed-speed wind turbines are low-cost, robust, reliable, simple to maintain, and proven in the field [2]. A large number of fixed-speed wind turbines have been installed over the past decade-and-a-half, and more continue to be installed [3]. While variable-speed wind turbines form the bulk of new installed capacity, a niche for fixed-speed wind turbines still exists. Therefore, it can be expected that

fixed-speed wind turbines will continue to play a role in the power systems of the future. While there are many wind turbine dynamic models available in the literature, the focus is largely on modeling variable-speed wind turbines [4–9]. These models often oversimplify the mechanical drive train and aerodynamics, since the aim is to evaluate power and rotor speed control mechanisms. In the model developed here, a modular approach is used to represent each of the turbine's functions. One block represents the aerodynamics, another the mechanical drive train, and a third represents the electrical generator. A control block may also be included. The blocks are integrated to form the complete wind turbine model, which is implemented in PSCAD/EMTDC and MATLAB/SIMULINK. This model is a platform on which more advanced variable-speed wind turbine models can be developed.

Variable-speed turbines use wound-rotor induction machines as generators, and control over output power is achieved through control of the rotor resistance, or through the use of power electronic converters in the rotor circuit in DFIG turbines. This chapter explains the principle behind rotor resistance control in detail, and discusses different control strategies for achieving optimal power extraction. The DFIG technology is also discussed and a model is developed and validated using available wind power plant field data.

## *1.3 Background on Wind Turbine Modeling*

Modeling of wind turbine generator systems (WTGS) can be broadly classified into:

1. Static modeling
2. Dynamic modeling

Static models of WTGS can be used for steady state analysis or quasi-steady state analysis such as load flow studies, power quality assessment, short circuit calculations whereas a dynamic model of WTGS is needed for various types of system dynamic analysis e.g. stability study, control system analysis, optimization techniques to mention just a few. Considering the static models of a WTGS, they are characterized by a simple voltage source (V), a voltage and real power source (V, P) or a real and reactive power source (P, Q). The choice of model used depends on specific application and the type of WTGS [10]. The tree diagram of Fig. 1 shows the model types and their applications. In this chapter the focus is on functional models designed for studying transient stability.

In general, a WTGS can be equipped with either a synchronous or asynchronous generator, it can be directly connected to the grid or connected through a power electronic converter. It may use aerodynamic torque control (blade pitching, stall control) and/or generator torque control (varying the rotor resistance, flux-vector control) for output power optimization. The possibilities stated give rise to a very general model framework, whose block diagram in shown in Fig. 2. This general framework is used to represent each wind turbine technology that is

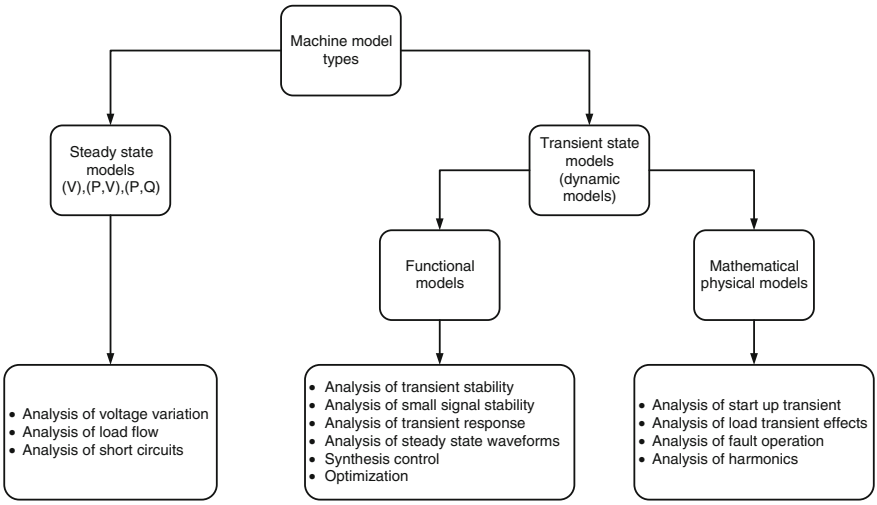


**Fig. 1** Model types and their applications

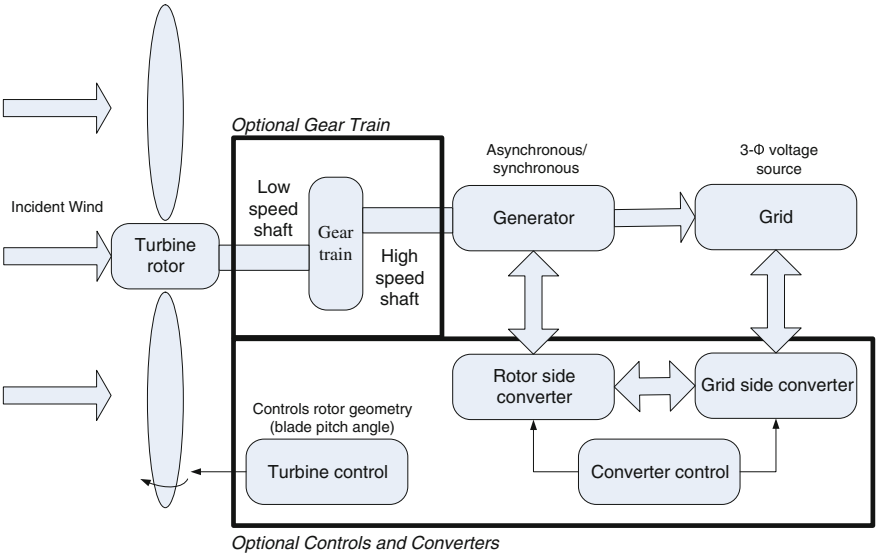


**Fig. 2** Functional block diagram for a generic wind turbine generator system

modeled in this chapter, with suitable modifications for each technology. This general framework is software-independent. In this chapter, each block of the framework is discussed. The physical theory behind each block is presented, and implementation of each block is also described. The development of the complete models is achieved by combining these blocks.

### 1.4 Chapter Organization

In the next section, the theory behind the blocks comprising the general framework is discussed. The following section describes the implementation of the wind turbine models for each of the three technologies mentioned previously, using the general framework. The implementation is carried out using PSCAD/EMTDC and MATLAB/SIMULINK platforms. The practical modeling issues, such as tuning of controllers for the various subsystems, are also discussed in this section. This section also includes the modeling of a DFIG WTGS with validation.

## 2 Modeling Concepts and Related Theory

Wind turbines are designed to capture the kinetic energy present in wind and convert it to electrical energy. An analogy can be drawn between wind turbines and conventional generating units which harness the kinetic energy of steam. From a modeling standpoint, a fixed-speed wind turbine consists of the following components:

1. Turbine rotor and blade assembly (prime mover)
2. Shaft and gearbox unit (drive-train and speed changer)
3. Induction generator
4. Control system

The interaction between each of the components listed above determines how much kinetic energy is extracted from the wind. Figure 3 illustrates the interaction between the wind turbine components in a basic fixed speed wind turbine. Modeling of the electrical subsystems is fairly straightforward, as power system modeling software usually includes a built-in induction machine model. However, modeling of the aerodynamics and mechanical drive-train is more challenging. These components are modeled based on the differential and algebraic equations that describe their operation. The following subsections describe the modeling of the four components listed above.

### 2.1 Aerodynamic Model

The aerodynamic block consists of three subsystems: tip-speed ratio calculation, rotor power coefficient ($C_p$) calculation, and aerodynamic torque calculation. Wind speed ($V_{wind}$) and pitch angle ($\beta$) are user-defined inputs. Since the model is intended to study the dynamic response of wind turbines to grid events, the assumption is usually made that the wind speed stays constant during the grid

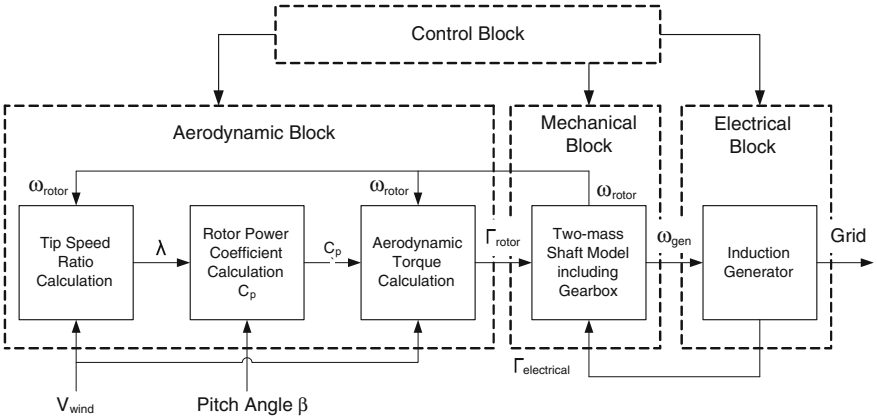


**Fig. 3** Block diagram for a fixed-speed stall-regulated wind turbine

event. However, the models allow the wind speed input signal to be set to any value at the start of the simulation run-time and also to be modified during the run. It is also possible to use a time-series of actual wind speed data.

### 2.1.1 Power Available in Wind Stream and its Extraction

The kinetic energy (KE) in any object of mass $m$ moving with a velocity $v$ is given by

$$KE = \frac{1}{2}mv^2 \tag{1}$$

A wind turbine is an electromechanical energy conversion device, that captures kinetic energy available from wind. This kinetic energy is turned into mechanical energy of the rotor and eventually into electrical energy from the generator. Power available in moving air is given as follows

$$P_{wind} = \frac{d(KE)}{dt} = \frac{1}{2}m'v^2 \tag{2}$$

where $m'$ is the mass flow rate. For a wind turbine rotor sweeping an area $A$ of radius $R$, power available in that area is given by Eq. (3)

$$P_{wind} = \frac{1}{2}\rho A v^3 \tag{3}$$

where $\rho$ is the air density, $A = \pi R^2$ and $v$ is the velocity of the moving air particles or in general wind. To determine the power extracted by a wind turbine rotor, Betz model (1926) is widely used. Betz model is not only used to find the power from an ideal turbine rotor, but also to find the thrust of the wind on the ideal rotor and

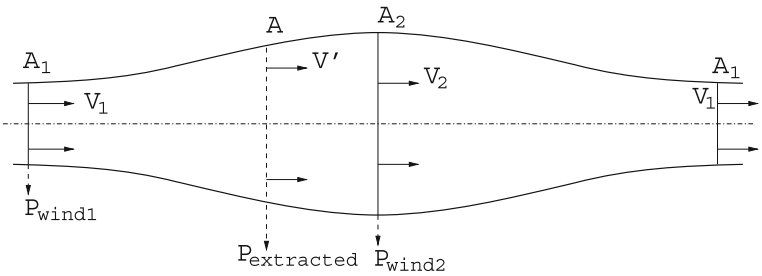


**Fig. 4** Wind flow conditions before and after the converter

the effect of the rotor operation on the local wind field. This simple model is based on linear momentum theory. The analysis assumes a control volume whose boundaries are the surface of a stream tube and its two cross sections. The turbine in the analysis is represented by a uniform *actuator disk* or *converter* which creates a discontinuity of pressure in the stream tube of air flowing through it. Betz analysis further assumes that [12].

- Air is homogeneous, incompressible and has achieved steady state fluid flow,
- There is no frictional drag,
- Number of blades on the rotor are infinite,
- Uniform thrust occurs over the disk or rotor area,
- A non-rotating wake, and
- The static pressure far upstream and far downstream of the rotor are equal to the undisturbed ambient static pressure;

Figure 4 shows the wind flow conditions for an energy converter. The power extracted from wind using such a converter, is given by the difference in moving air particle power before and after the converter. The power extracted by the energy converter is given by Eq. (4)

$$P_{extracted} = P_{wind1} - P_{wind2} = \frac{1}{2}\rho(A_1 v_1^3 - A_2 v_2^3) \tag{4}$$

Figure 4 describes the change in wind velocity before and after the converter. To achieve ideal efficiency in energy conversion it is required that the air velocity after the converter ($v_2$) becomes zero. This is physically impossible, because that would render a need for the wind velocity before the converter to be zero and the air to be still. A more practical energy converter, will have air pressure increase just before the converter, which would simultaneously result in air velocity decrease, thus exerting a force given by Eq. (5)

$$F = m'(v_1 - v_2) \tag{5}$$

Thus, the power extracted from wind is given by Eq. (6)

$$P_{extracted} = Fv' = m'(v_1 - v_2)v' \tag{6}$$

By comparing the two equations obtained for $P_{extracted}$ [Eqs. (4)–(6)], and assuming that the mass flow rate through the converter is constant, the air velocity through the converter is the average wind velocity $v' = \frac{1}{2}(v_1 + v_2)$. Then the power extracted from the converter can be computed as

$$P_{extracted} = \frac{1}{4}\rho A(v_1^2 - v_2^2)(v_1 + v_2) \tag{7}$$

The term rotor power coefficient can now be defined (since, $P_{extracted} < P_{wind}$) as follows

$$C_p = \frac{P_{extracted}}{P_{wind}} \tag{8}$$

It is the ratio of power extracted from the rotor to the power available from wind, also known as rotor performance coefficient and sometimes referred as Betz factor. As described earlier, Betz created a (1D) model based on linear momentum theory, along with some assumptions for the analysis. The power coefficient can achieve a maximum value of 0.593, when $\frac{v_2}{v_1} = \frac{1}{3}$. This is the maximum theoretically possible value of $C_p$. Due to aerodynamic losses, actual value of power coefficient never achieves 0.593. In practice three effects are accounted for decrease in maximum achievable value of $C_p$.

1. Rotation of wake behind the rotor
2. Finite number of possible rotor blades and their associated tip losses, and
3. Non-zero aerodynamic drag [12]

In the next section, the relation between $C_p$ and tip speed ratio ($\lambda_r$) at a particular value of blade pitch angle ($\beta$) will be presented. This relation can be used to develop $C_p - \lambda_r$ curves. These are used to determine the rotor power for any combination of wind speed and rotor speed. These curves provide immediate information on the maximum value of $C_p$ and optimum tip speed ratio. The data for such a relationship is found from turbine tests and modeling [12].

### 2.1.2 Relation of Power Coefficient with Pitch Angle and Tip Speed Ratio

An empirical relation between $C_p$ (rotor power coefficient), tip speed ratio ($\lambda_r$) and blade pitch angle ($\beta$) is used for developing a look-up table that provides a value of $C_p$ for a given value of wind speed and tip speed ratio. Blade pitch angle can be defined as the angle between the plane of rotation and blade chord line. Tip speed ratio is defined as the ratio of the blade-tip linear speed to the wind speed [12]

$$\lambda_r = \frac{\omega_{rot} R}{v_1} \tag{9}$$

where $R$ is the rotor radius and $\omega_{rot}$ is the angular velocity of the rotor.

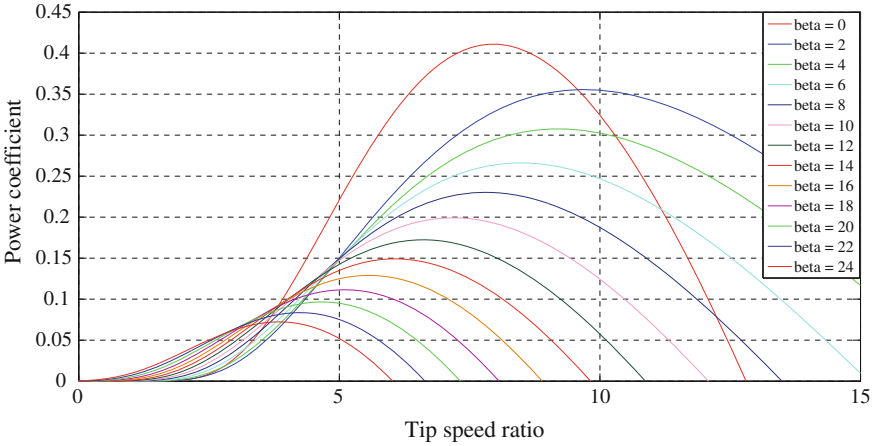


**Fig. 5** Power coefficient $C_p$ as a function of tip speed ratio $\lambda_r$

Shown below is one such empirical relation between $C_p$, $\lambda_r$, and $\beta$. Equation (10) is used to generate a look-up table for $C_p$. When provided with the values of $\lambda_r$ and $\beta$, the corresponding value of $C_p$ can be found. The $C_p(\lambda_r)$ curve obtained from the equation works only for positive values of pitch angle $\beta$.

$$C_p(\lambda, \beta) = c_1\left(c_2\frac{1}{\Lambda} - c_3\beta - c_4\beta^x - c_5\right)e^{-c_6\frac{1}{\Lambda}} \tag{10}$$

$$\frac{1}{\Lambda} = \frac{1}{\lambda + 0.08\beta} - \frac{0.035}{1+\beta^3} \tag{11}$$

while the coefficients $c_1 - c_6$ are proposed as equal to : $c_1 = 0.5, c_2 = 116, c_3 = 0.4, c_4 = 0, c_5 = 5, c_6 = 21$ [10]. Once, $C_p$ is determined, aerodynamic torque of the rotor can be computed using Eqs. (3), (8) and (12). A mechanical model for the drive train developed in next Sect. 2.1.3 is used to determine the angular speed of the generator, $\omega_{gen}$ and angular speed of the turbine rotor, $\omega_{rot}$. For all the models developed $\omega_{gen}$ is provided as an input to the induction machine.

$$P_{extracted} = \tau_{rot}\omega_{rot} \tag{12}$$

Figure 5 shows the $C_p$ versus $\lambda_r$ characteristics obtained from Eq. (10), note that only positive values of blade pitch angle can be used with these curves.

### 2.1.3 Blade Pitching

Blade pitch angle control is used to directly vary the power coefficient of a wind turbine. As it determines the operating power coefficient, it can be effectively used to control the mechanical output power of the rotor. A reduction in mechanical

power of the rotor can be achieved by reducing or minimizing the angle of attack above its critical value. By limiting the power coefficient, power extracted from the wind is limited. This kind of power control is also known as *pitch control*. Pitch control can be used to serve different purposes such as

- Optimizing the power output of the wind turbine, by maximizing the mechanical power output for a given wind speed, this is generally applied for low and moderate wind speeds below rated wind speed.
- Preventing excess mechanical power output in strong winds above rated wind speeds. This keeps a check on the mechanical power and keeps it below the rated value in strong winds.
- To prevent disconnected wind turbines from turning [11].

There are two common ways in which pitch angle control can be used for regulating the power output of wind turbines

- Active pitch control: For variable-speed pitch-regulated wind turbines, wind turbine operation and power output can be affected either by speed changes or blade pitch angle changes. Below rated power, such machines operate at variable speed to optimize the tip speed ratio at fixed pitch. After rated power output is achieved generator torque control is used to maintain output power, while pitch control is used to maintain rotor speed. At high wind speeds, power output of the generator can be maintained constant, with an increase in rotor speed. This increased energy available from the wind is stored as kinetic energy in the rotor. This results in reduced aerodynamic torque and thus deceleration of the rotor. If the wind speed continues to remain high, aerodynamic efficiency of the rotor can be reduced by changing the pitch, resulting in reduced rotor speed.
- Passive pitch control : In case of passive control wind speed is used to provide the actuator power, which adjusts the blade pitch angle to shape the power curve of the wind turbine. In such wind turbine designs, the effects of change in rotor speed or wind speed are related to change in blade pitch angle.

## *2.2 Mechanical Drive Train Model*

The drive train of a wind turbine generally consists of turbine rotor, low speed rotor shaft, gearbox with transmission ratio $a$, high speed shaft of the generator and the generator itself (either synchronous or induction). In case of wind turbines using synchronous generators, usually the design calls for a generator with a high pole count, thus reducing the mechanical speed of the generator shaft. The gearbox can then be omitted from the drive train. More than 90 % of the drive train moment of inertia is accounted for by the rotor (blades and hub) [10]. The generator accounts for 6–8 %, while the remaining parts account for 2–4 % of the total moment of inertia. Since the generator's torsional stiffness is very high, approximately two orders of magnitude higher than that of the rotor shaft, and

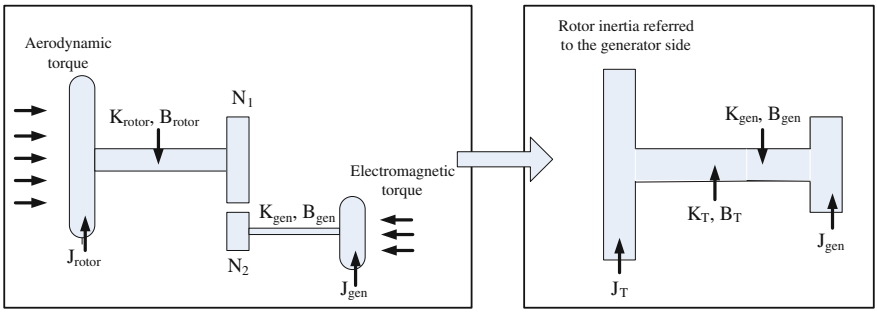


**Fig. 6** Two-mass model for the drive train

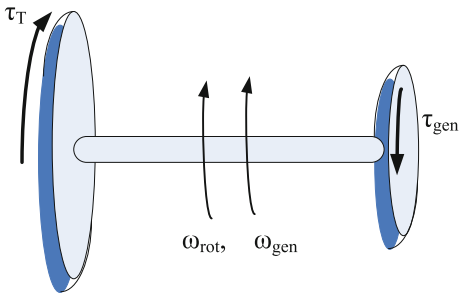


**Fig. 7** Two-mass model for the drive train with opposing torque action

about fifty times higher than the hub with blades, the torsional vibration on the drive train elements cannot be ignored. Their characteristics (frequency and amplitude) can affect wind turbine performance. Hence, it is impossible to model the drive train as a lumped single mass. Typically the masses of the rotor and the generator are much larger than the mass of the gearbox. If we neglect the mass of the gearbox, the properties (stiffness constant and torsional constant) of the two shafts can be combined into one equivalent shaft resulting in a two-mass model as shown in Fig. 6. Moreover, the equivalent shaft of the two-mass model is not infinitely stiff, and thus the model cannot be generally reduced to a one-mass model. Hence, a *two-mass* model is preferred.

Note from Fig. 7 that the aerodynamic torque from the rotor is counteracted by the electromagnetic torque from the generator. Also note from Fig. 6 that rotor speed $\omega_{rot}$, torque $\tau_{rot}$ and moment of inertia $J_{rot}$ are all referred to the generator side using the gear transmission ratio $a$.

By balancing the torque for each mass, differential equations formed can be solved to determine the rotor, generator speeds $\omega_{rot}$ and $\omega_{gen}$ respectively. For each rotating mass, the product of moment of inertia $J$ and angular acceleration $\theta''$ must equal the sum of the torques acting on the mass.

For the turbine rotor torque, equation can be written as

$$J_T\theta_T'' = \tau_T - B_{eqv}(\omega_T - \omega_G) - K_e qv(\theta_T - \theta_G) \tag{13}$$

For the generator torque, equation can be written as

$$J_G\theta''_G = -\tau_G + B_{eqv}(\omega_T - \omega_G) + K_e qv(\theta_T - \theta_G) \quad (14)$$

subscript T used in Eqs. (13) and (14) denotes the rotor parameters referred to the generator side of the gearbox and subscript G denotes generator parameters.

## 2.3 Modeling of Induction Machines

The induction machine has typically been favored for use in wind turbines due to the fact that induction generators do not need to be synchronized with the grid. Since wind turbines operate under varying wind speed conditions, resulting in varying shaft speeds, conventional synchronous generators cannot be easily used for this application. In a conventional synchronous machine connected to a steam turbine, it is possible to control real and reactive power output independently of each other by varying the steam flow rate and the excitation respectively. This decoupling effect cannot be achieved in fixed-speed and rotor-resistance control based technologies. In a DFIG turbine, the decoupling of real and reactive power is achieved through the use of power electronics and flux-vector control. In this subsection the considerations for modeling an induction machine and the concept of flux-vector control are introduced.

### 2.3.1 Introduction

The winding arrangement of a conventional 2-pole, 3-phase, wye-connected symmetrical induction machine is shown in Fig. 8. The stator windings are identical with equivalent turns $N_s$ and resistance $r_s$. The rotor windings can be approximated as identical windings with equivalent turns $N_r$ and resistance $r_r$. The model assumes the air-gap is uniform and the windings are sinusoidally distributed.

In Fig. 8, the winding of each phase is represented by an elementary coil. One side of the coil is represented by a $\otimes$ indicating that the assumed positive direction of current is down the length of the stator (into the plane of the paper). The other side of the same coil is represented by a $\odot$ which indicates that the assumed positive direction of current is out of the plane of the paper. The axes *as*, *bs* and *cs* represent the positive directions of the magnetic fields produced due to the currents flowing in the stator windings of phase *a*, *b* and *c* respectively. These directions are obtained using the right hand rule on the phase windings. Similarly axes *ar*, *br* and *cr* with respect to the rotor windings are shown. These rotor axes are fixed to the rotor and rotate with it at an angular velocity of $\omega_r$. The angular displacement of the rotor with respect to the positive *as* axis is $\theta_r$. In the stationary *abc* reference frame, the relationships between voltages, currents and flux linkages of each phase for this machine can be written from Fig. 9.

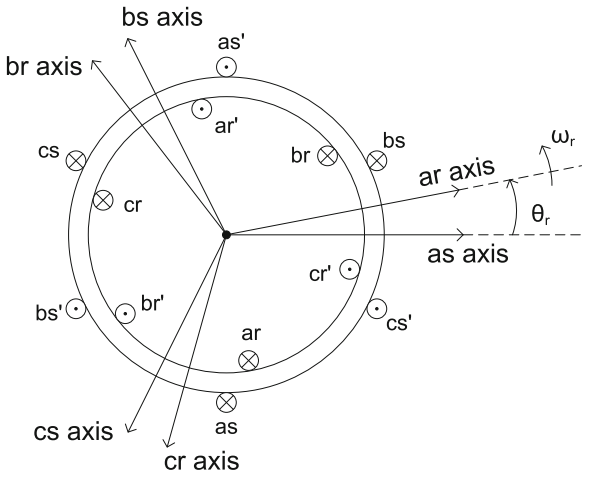


**Fig. 8** Schematic winding diagram

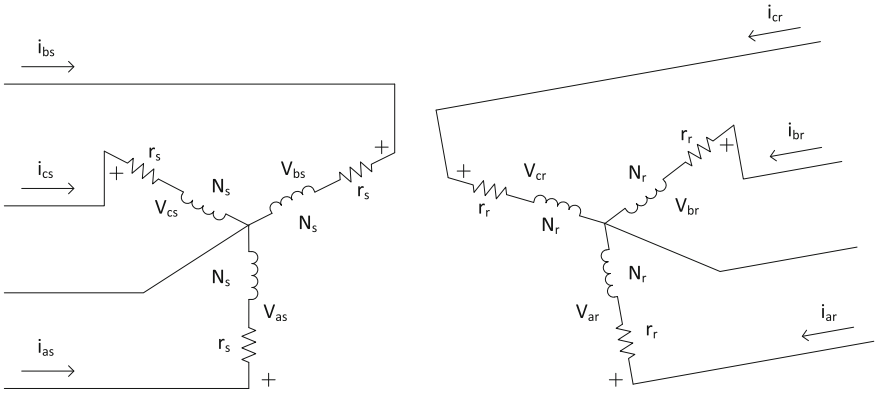


**Fig. 9** Equivalent circuit (2-pole, 3-phase, wye-connected IM)

### 2.3.2 Reference Frame Theory and the Clarke and Park Transforms

It is known that for rotating machine inductances are functions of the rotor speed, due to which the coefficients of the differential equations (voltage equations) describing machine operation vary with time, except when the rotor is stationary. It is difficult to develop machine models that can be used for dynamic studies, using these complex equations. These time-varying equations can be written in a time-invariant form by choosing a frame of reference that is rotating at the appropriate speed. Referring machine variables to a rotating frame can, not only reduce the complexity of modeling the machine but also serve as a tool for better understanding of machine operation. Two such transformations to be used for

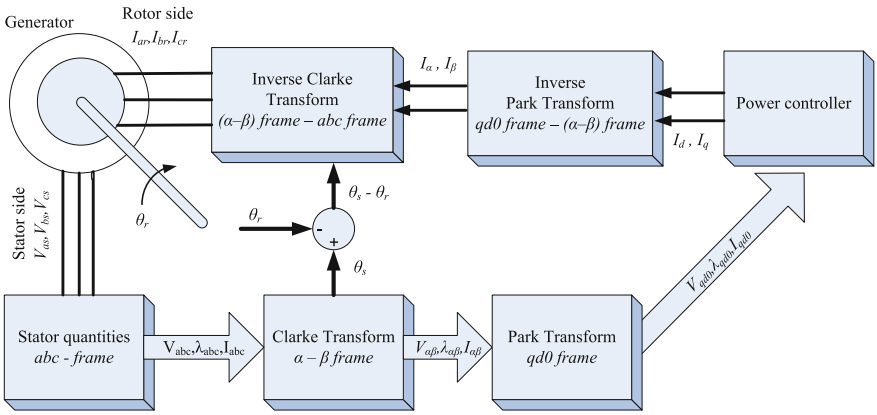


**Fig. 10** Block diagram for abc-$\alpha\beta$-qd0 transform used for DFIG

developing a doubly-fed induction generator based wind turbine model are the Clarke and Park transforms. These are two different transformations used to achieve independent active and reactive power control for induction generators. When used in conjunction, these transforms convert stator *abc* quantities to $\alpha - \beta$ quantities (stationary two axis frame also known as $(\alpha - \beta)$ frame—Clarke transform) and eventually to the rotating *qd0* frame (Park Transform) as shown in Fig. 10.

### Transformation from *abc* Frame to *qd0* Frame

In the stationary *abc* reference frame, the relationships between the voltages, currents and flux linkages of each phase for an induction machine can be written as follows:

$$\vec{V}_{abcs} = \vec{r}_s \vec{i}_{abcs} + \frac{d(\vec{\lambda}_{abcs})}{dt} \tag{15}$$

$$\vec{V}'_{abcs} = \vec{r}_s \vec{i}'_{abcs} + \frac{d(\vec{\lambda}'_{abcs})}{dt} \tag{16}$$

where, $\lambda$ is the flux linkage, subscripts s and r stand for variables and parameters associated with the stator and rotor side respectively, Eq.(16) represents machine parameters when referred to the rotor side. The flux linkages in the Eqs. (15)–(16) can be written as

$$\vec{\lambda}_{abcs} = \vec{L}_{sr} \vec{i}_{abcs} + \vec{L}'_{sr} \vec{i}'_{abcr} \tag{17}$$

$$\vec{\lambda}'_{abcr} = \vec{L}'^{T}_{sr} \vec{i}_{abcs} + \vec{L}'_{r} \vec{i}'_{abcr} \tag{18}$$

The resultant voltage equations from Eqs. (15)–(18) are as follows

$$\vec{V}_{abcs} = \left(\vec{r}_s + \frac{d\vec{L}_{sr}}{dt}\right)\vec{i}_{abcs} + \frac{d\vec{L}'_{sr}}{dt}\vec{i}_{abcr} \tag{19}$$

$$\vec{V}'_{abcr} = \frac{d\vec{L}'^{\mathrm{T}}_{sr}}{dt}\vec{i}_{abcs} + \left(\vec{r}'_r + \frac{d\vec{L}'_r}{dt}\right)\vec{i}_{abcr} \tag{20}$$

As can be seen in Eqs. (19) and (20) voltages, inductances and currents are in the stationary *abc* reference frame. They are thus time-variant. Analysis and modeling of time-variant equations is cumbersome. Using the Clarke and Park transforms these time-variant quantities can be converted into time-invariant quantities. Applying Park transform, the *abc* frame quantities are converted in *qd*0 frame quantities. *qd*0 frame is rotating at the synchronous frequency.

$$\vec{V}_{qd0s} = \vec{r}_s\vec{i}_{qd0s} + \omega_{qds}\vec{\lambda}_{dqs} + \frac{d\vec{\lambda}_{qd0s}}{dt} \tag{21}$$

$$\vec{V}'_{qd0r} = \vec{r}'_r\vec{i}_{qd0r} + (\omega_s - \omega_r)\vec{\lambda}'_{dqr} + \frac{d\vec{\lambda}'_{qd0r}}{dt} \tag{22}$$

where $\omega_s$ and $\omega_r$ are the rotational speed of the synchronously rotating *qd*0 frame and rotor frame respectively.

A wound rotor induction machine can be represented in a synchronously rotating *qd*0 reference frame as described above. Assuming that the stator currents are balanced, a resultant stator magnetic field ($H_{total}$) with a constant magnitude and rotating at synchronous speed ($\omega_s$) is produced [13]. Using Clarke's transform, $\theta_s$ can be obtained and *qd*0 frame rotated at synchronous speed $\omega_s$. Now, since the angular speeds of the stator magnetic field and the *qd*0 rotating frame are identical, stator magnetic field vector $\vec{\lambda}_{total}$ is fixed with respect to the *q*- and *d*-axes of the *qd*0 rotating frame. If the *q*-axis of the rotating *qd*0 frame is oriented in such a manner, so that it aligns perfectly with the $\vec{\lambda}_{total}$, field along the *q*-axis would be of zero magnitude. Figure 11 shows MATLAB plots for the stator magnetic field in stationary *abc*, $\alpha\beta$ and rotating *qd*0 frames. Figure 12 shows the alignment of equivalent stator flux along the *q*-axis.

Since, $\lambda_{total}$ is aligned along the *q*-axis,

$$\lambda_{qs} = \lambda_{total} \tag{23}$$

and

$$\lambda_{ds} = 0 \tag{24}$$

substituting Eqs. (23)–(24) in Eqs. (21)–(22), $V_{ds}$ and $V_{qs}$ are obtained

$$V_{ds} = -\omega_s\lambda_{qs} = \omega_s\lambda_{total} = constant \tag{25}$$

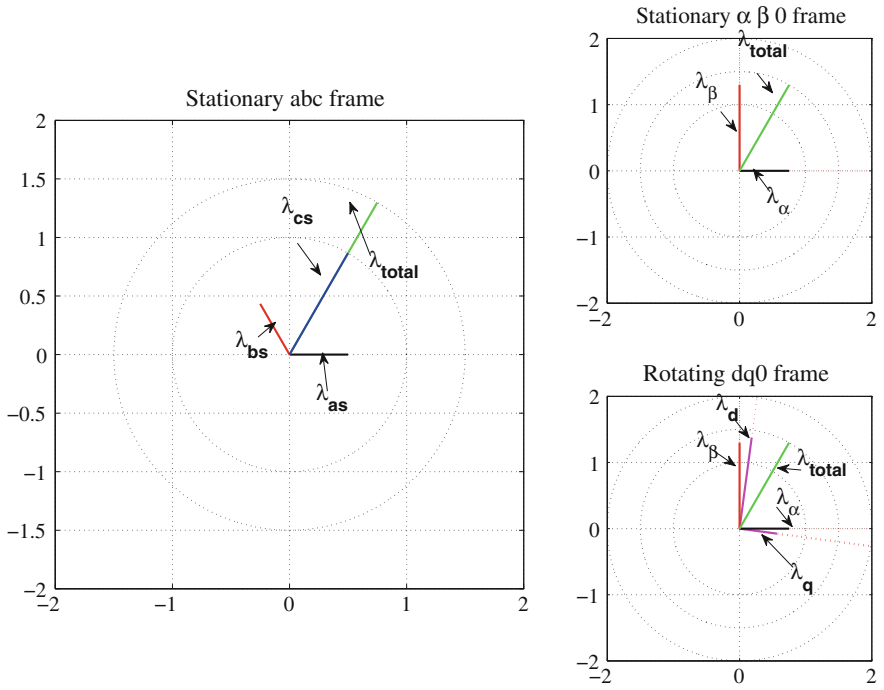


**Fig. 11** Transformation from *abc* to *rotating qd*0 frame

and

$$V_{qs} = 0 \tag{26}$$

From Eq. (25) speed of the stator field $\omega_s$ is constant, hence $V_{ds}$ is time invariant and $V_{qs}$ is almost negligible, with $\lambda_{ds} = 0$, the stator $q$-axis current can be obtained as

$$i_{qs} = \frac{\lambda_{qs} - L_m i'_{qr}}{L_{ls} + L_M} \tag{27}$$

Similarly, the stator $d$-axis current can be obtained as

$$i_{ds} = \frac{-L_m i'_{dr}}{L_{ls} + L_M} \tag{28}$$

From these results it can be seen that the stator currents are linearly dependent on the rotor currents. Inductance and flux quantities in Eqs. (27) and (28) are time-invariant, thus the stator $qd$0 axis currents can be controlled by adjusting the rotor $q$-axis and $d$-axis currents appropriately. The next step is to show that the real and reactive power output of the machine can be decoupled, and control over real and reactive power can be achieved through controlling rotor $q$- and $d$-axis currents

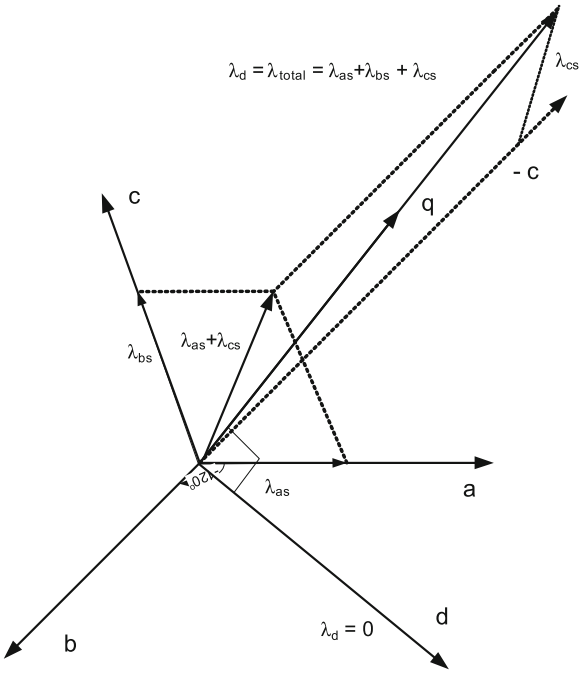


**Fig. 12** Aligning equivalent stator flux $\lambda_{\text{total}}$ along $q$-axis

respectively. The real and reactive power in the stator windings can be derived as follows:

$$S = V_s I_s^* \tag{29}$$

$$V_s = V_{qs} + jV_{ds} \tag{30}$$

$$I_s = I_{ds} + jI_{qs} \tag{31}$$

Thus, apparent power $S$ is given by

$$S = P_s + jQ_s = (V_{qs}I_{ds} + V_{ds}I_{qs}) + j(V_{ds}I_{ds} - V_{qs}I_{qs}) \tag{32}$$

$$P_s = \frac{3}{2}(V_{qs}i_{ds} + V_{ds}i_{qs}) \tag{33}$$

$$Q_s = \frac{3}{2}(V_{ds}i_{ds} - V_{qs}i_{qs}) \tag{34}$$

Since, $V_{qs} = 0$, Eqs. (33) and (34) can be written as

$$P_s = \frac{3}{2}V_{ds}i_{qs} \tag{35}$$

$$Q_s = \frac{3}{2} V_{ds} i_{ds} \tag{36}$$

From Eqs. (35), (36), (27) and (28) active and reactive power equations can be simplified as follows

$$P_s = \frac{-3}{2} \omega_s \lambda_{qs} \left( \frac{\lambda_{qs} - L_m i'_{qr}}{L_{ls} + L_M} \right) \tag{37}$$

$$Q_s = \frac{3}{2} \omega_s \lambda_{qs} \left( \frac{L_m i'_{dr}}{L_{ls} + L_M} \right) \tag{38}$$

From Eqs. (37)–(38) it can be noted that, quantities like $\lambda_{qs}$, $\omega_s$, $L_{ls}$, $L_M$, $L_m$ are all time invariant quantities, thus Eqs. (37)–(38) can be further simplified as

$$P_s = (k_{ps1} - k_{ps2}) i'_{qr} \tag{39}$$

$$Q_s = k_{qs} i'_{dr} \tag{40}$$

where $k_{ps1}$, $k_{ps2}$, $k_{qs}$ are the respective constants of active and reactive power equations. It can be clearly seen from Eqs. (39)–(40) that stator active power $P_s$ can be independently controlled by $q$-axis rotor current, while stator reactive power $Q_s$ can be independently controlled by $d$-axis rotor current in an induction machine.

## 3 Wind Turbine Model Development and Implementation

This section describes wind turbine models developed in PSCAD/EMTDC and MATLAB/SIMULINK platforms. The first model developed was a fixed speed wind turbine model, it produces rated active power at rated wind speed (one wind speed only). As the wind turbine operates at a constant angular speed (rpm), maximum power is obtained at one wind speed only. It should be noted that blade pitch angle is kept constant for the model. Hence, the efficiency of such a wind turbine at varying wind speeds is less. The blade pitch angle for such wind turbines is a preset value, determined by wind speed in the area of installation. The blade pitch angle at which maximum power is obtained varies for different $C_p$ versus $\lambda_r$ characteristics. For simulation purposes, the rated wind speed was set at 14 m/s, with cut-in speed of 6 m/s and cut-out speed of 20 m/s. The blade pitch angle was set to $-6.1667°$. With the basic model at hand, fixed speed model is further developed into a variable speed wind turbine model [14]. The advantage of a variable speed wind turbine is that, the torque speed characteristics of the machine can be manipulated, to obtain maximum/rated power at varying wind speed. To put it very precisely, a variable speed wind turbine has larger generator speed

variations than the fixed speed wind turbine. It is capable of producing maximum torque, thus maximum power at different generator speeds.

To achieve rated power output above rated wind speed, different control strategies are implemented. Now, rated power above rated wind speed can be produced in two ways

- Pitch control
- Rotor resistance based control

In case of the first method, the operating, blade pitch angle is varied to obtain rated power at any wind speed above rated, this method does not manipulate the torque speed characteristics of the machine. It can be visualized as fixed speed wind turbine, which operates at variable pitch angles achieved by calculating the optimum pitch angle for a given wind speed and output power, and then physically changing the rotor blade pitch angle, while the turbine is in operation. The second method entails, more control over the torque speed characteristics of the machine, as the rotor resistance is varied, generator speed changes, and the machine operates with new torque speed curve depending on the output torque and thus the power requirement.

As discussed earlier, in case of utilizing an induction machine for wind turbines, it can be directly connected to the grid, or through a power electronic converter. When the rotor and stator side of the machine are switched using converters (rectifier and inverter), such a system is called doubly-fed induction generator system (DFIG). Using a DFIG provides independent active (P) and reactive (Q) power control of the machine. When using a variable-speed rotor resistance control or variable-speed pitch control strategy, desired active power can be obtained, but there is no control over the reactive power absorbed or generated by the machine. In further sections, a detailed model development procedure for fixed speed, variable speed and DFIG based wind turbine system has been discussed. Given below is a list of wind turbine models. All models employ induction machine, which is rated at $V_{ll} = 690$ V, S $= 1.8$ MVA. A detailed machine specification including stator and rotor resistances and inductances can be found in the appendix section. The rated power output of the turbine was set to 1.5 MW.

The different configurations of wind turbine models, that were implemented are listed below

- Fixed speed wind turbine model
- Variable speed wind turbine model
  - Rotor resistance control

    Constant power strategy
    Constant current strategy
- Doubly Fed induction generator model

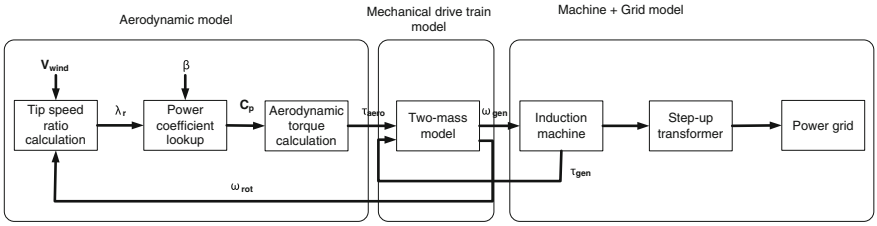


**Fig. 13** Generic model for fixed speed wind turbine

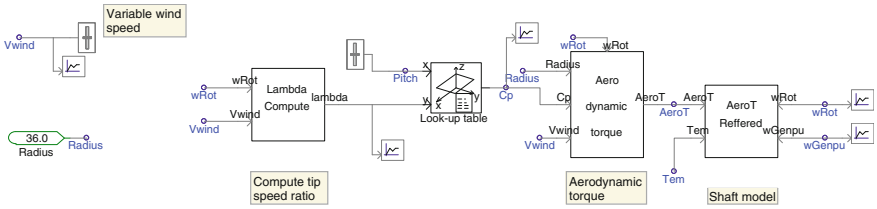


**Fig. 14** PSCAD simulation model for a WT

## *3.1 Fixed Speed Wind Turbine*

For fixed speed wind turbine, over the entire wind sweep from cut-in speed of 6 m/s to cut-out speed of 20 m/s, generator speed does not vary much, hence the name *fixed speed wind turbine*. The aerodynamic model developed for a fixed speed wind turbine, is used for all the other wind turbine models. The only function of the aerodynamic model is to provide the speed input to the generator. As the generator speed input varies with wind speed, the power output of the generator varies accordingly. In case of the fixed speed wind turbine, the output power profile builds up with increase in wind speed from cut-in wind speed of 6 m/s, peaks at 14 m/s (rated wind speed) and then drops later due to passive stalling of the rotor blades. Figure 13 shows the specific block diagram representation of the fixed speed wind turbine which is modeled, based on the more general diagram given in Fig. 3. Figure 14 shows the simulation model components in PSCAD.

### 3.1.1 Fixed-Speed Wind Turbine Model in PSCAD/EMTDC

As can be seen from the block diagram, wind speed variable $V_{wind}$ and rotor speed $\omega_{rot}$ are used to compute the tip speed ratio ($\lambda_r$) given by the relation in Eq. (9), where $R = 36$ m. Using $\lambda_r$ and the a blade pitch angle as inputs to a lookup table, corresponding value of power coefficient ($C_p$) is computed. The relation between $C_p$, $\lambda_r$ and blade pitch angle ($\beta$) used for all models are given in Eqs. (10) and (11). The $C_p$ versus $\lambda_r$ characteristics obtained are shown in Fig. 5. Once, $C_p$ is

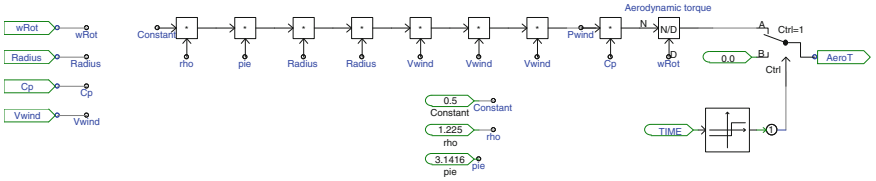


**Fig. 15** Aerodynamic torque computation

obtained, it is then used by the aerodynamic torque calculation block to calculate the instantaneous aerodynamic torque of the rotor. Shown in Fig. 15 is the internal block diagram of the aerodynamic torque calculation block.

Since, the rotor shaft is a low speed shaft rotating between 15 and 20 rpm, a gear train has to be included, which is then connected to the high speed shaft of the induction generator rotating at a base frequency of 125.667 rad/sec, for a 6 pole machine converts to 1,200 rpm. To model the gear train, incorporating the rotor slow speed shaft, gear train and generator high speed shaft as a two-mass model. The two-mass model is governed by three differential equations, Eqs. (41), (42) and (48) and a gear ratio of $a = 70$ was assumed. A detailed list of constants used for modeling the gear train and the rotor, generator shafts is provided in the Appendix section. Given below is the set of differential equations used to model the gear train and rotor generator shafts as a two-mass.

$$\frac{dX_1}{dt} = \omega_{rotr} - \omega_{gen} \tag{41}$$

$$\frac{d\omega_{rotr}}{dt} = \frac{\tau_{aeror} - B_{eqv}(\omega_{rotr} - \omega_{gen}) - K_{eqv}X_1}{J_{rotr}} \tag{42}$$

$$\frac{d\omega_{gen}}{dt} = \frac{-\tau_{gen} - B_{eqv}(\omega_{rotr} - \omega_{gen}) + K_{eqv}X_1}{J_{gen}} \tag{43}$$

$$J_{rotr} = \frac{J_{rot}}{a^2} \tag{44}$$

$$B_{eqv} = \frac{B_{rot}}{a^2} + B_{gen} \tag{45}$$

$$K_{eqv} = \frac{\frac{K_{rot}}{a^2}K_{gen}}{\frac{K_{rot}}{a^2} + K_{gen}} \tag{46}$$

Equations (41), (42) and (48) can be solved with initial conditions of the integrator set for $\omega_{rot} = \omega_{gen} = 125.66$ rad/sec from Eq. (47), (48). $\tau_{aeror}$ is the aerodynamic torque referred to the generator shaft, obtained by dividing it by the gear ratio. $J_{rotr}$ is the moment of inertia of the rotor referred to the generator shaft. Electromagnetic torque output of the induction machine $\tau_{gen}$ is converted from its per unit equivalent by multiplying it by the rated generator torque = 15,914.67 Nm

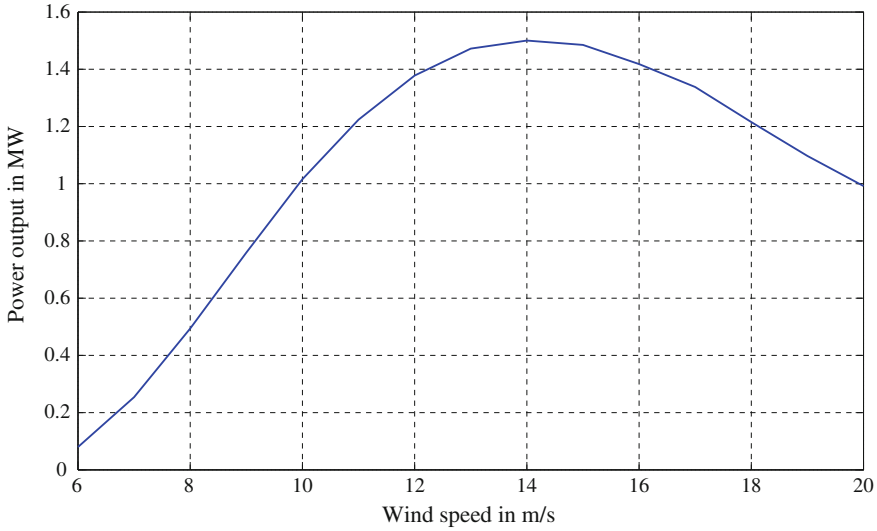


**Fig. 16** Power profile for fixed speed wind turbine model

[refer Eq. (12)]. A negative value of $\tau_{gen}$ is applied to the two-mass model, as it operates against the rotor torque. Before feeding $\omega_{gen}$ to the machine, it is converted to its per unit equivalent by dividing it by the rated speed of 125.667 rad/sec.

$$N = \frac{120f}{P} \tag{47}$$

$$\omega_{gen} = \frac{2\pi N}{60} \tag{48}$$

where $N$ is the generator speed in rpm, $P$ is the number of poles and $f$ is the synchronous frequency.

The PSCAD machine model is directly connected to the grid. A step up transformer connected in *delta−wye* is used to connect the stator terminals to a three-$\phi$ voltage source (representing the grid). Once the model is ready, the blade pitch angle has to be set to obtain rated power of 1.5 MW. It was observed that, a maximum power of 1.5 MW was obtained at $\beta = -6.166°$. $\beta$ is then kept fixed and rated wind speed is set at which machine outputs 1.5 MW. The model is then run at wind speed ranging from 6 to 20 m/s. The power profile for the model is then obtained as shown in Fig. 16.

A look at the power profile of the wind turbine shows that rated power of 1.5 MW is obtained at a fixed wind speed of 14 m/s and, fixed pitch of −6.166°. As the wind speed varies power produced varies roughly as the cube of the wind speed. At rated wind speed the electrical power generated becomes equal to the rating of the turbine, and then stalling takes place above the rated wind speed. This is achieved by making use of post-stall reduction in lift coefficient and associated

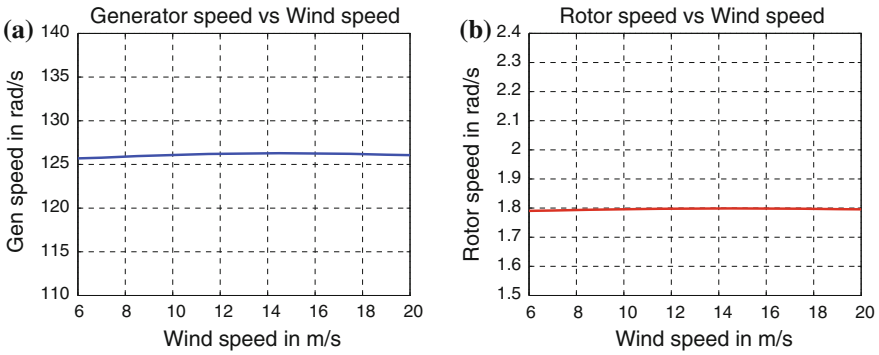


**Fig. 17** Rotor and generator speed variation with wind speed. **a** Generator speed variation with wind speed. **b** Rotor speed variation with wind speed

increase in drag coefficient, which places a ceiling on the output power as wind speed increases. As can be seen from Fig. 16 power output of the generator falls below 1.5 MW at any wind speed above 14 m/s. It can be also noted that, the output of the generator drops significantly almost 0.079 MW at a wind speed of 6 m/s. This stalling of the wind turbine is attributed to the increase in angle of attack as wind speed increases, and increasingly large part of the blade enters the stall region. The stalling effect reduces the rotor efficiency and puts a cap on the output power. Stall regulated machines generally suffer from the disadvantage of uncertainties in aerodynamic behavior post-stall, which can result in inaccurate power levels and blade loading at rated wind speed and above.

For a fixed speed wind turbine, rotor speed and thus the generator speed variation as wind speed varies are very less. As can be seen from Fig. 17a, b, the generator speed reaches a maximum of 126.281 rad/sec at 14 m/s and then decreases due to passive stalling. The overall slip variation is a maximum of −0.49 %. Results obtained from the PSCAD model are later compared with those from a similarly developed MATLAB/SIMULINK model to demonstrate that the model can be implemented in different platforms.

A torque *Vs* slip plot for the model shows that, the torque rise is very steep. As the wind speed increases, the generator speed does not increase, as shown in Fig. 17a it attains a maximum value at 14 m/s. The generator torque achieves maximum value at 14 m/s and then drops above rated speed. Figure 18 shows the torque slip characteristics of the machine during the entire wind speed sweep from 6 to 20 m/s.

### 3.1.2 Fixed-Speed Wind Turbine Model in MATLAB/SIMULINK

For the purpose of demonstrating the generality of the model shown in Fig. 13, the results obtained from the PSCAD/EMTDC model of fixed speed wind turbine are compared with those from a parallel MATLAB/SIMULINK model. A similar approach for modeling the wind turbine was used. Initially an aerodynamic model

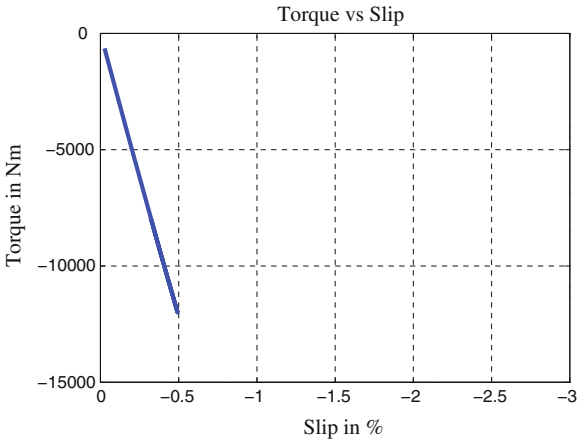


**Fig. 18** Torque slip characteristics

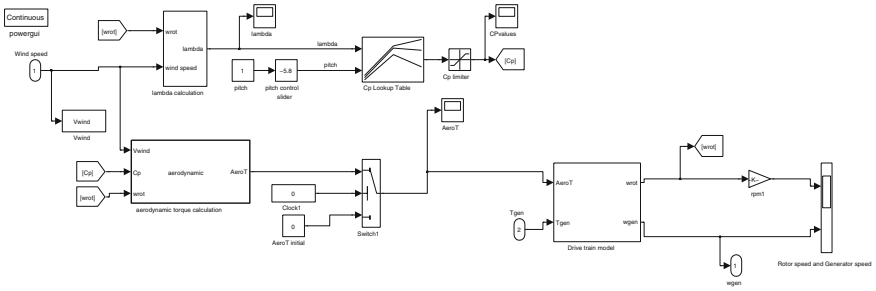


**Fig. 19** Aerodynamic model in SIMULINK

simulating the rotor blades, rotor shaft, gear train and generator shaft was modeled in SIMULINK. Generator speed output $\omega_{gen}$ was then fed to a induction machine model, working in the squirrel cage mode (rotor circuit shorted). The built-in machine model in SIMULINK provides a number of options for machine specifications. The machine can be customized very well according to the model demand. It provides a greater depth in terms of setting the reference frame with options of stationary, synchronous and rotor frames. The machine stator is connected to a three phase RLC voltage source through a *delta-wye* connected 0.69/34.5 kV step up transformer. X/R ratio for the voltage source is set at 10. Figure 19 shows the internal block diagram for the aerodynamic model developed in SIMULINK. The results from both the models were seen to match closely.

The aerodynamic model in Fig. 20 is provided a ramp input for wind speed, the simulation time is set for 100 s with a ramp rate of 0.14 m/s$^2$, with an initial wind speed of 6 m/s, which means that at 100 s, the wind speed reaches a peak of 20 m/s. The rotor blade pitch angle is set to −5.8° and an empirical lookup table is used to determine $C_p$ using tip speed ratio ($\lambda$) and pitch angle ($\beta$) as inputs. Once, $C_p$ is

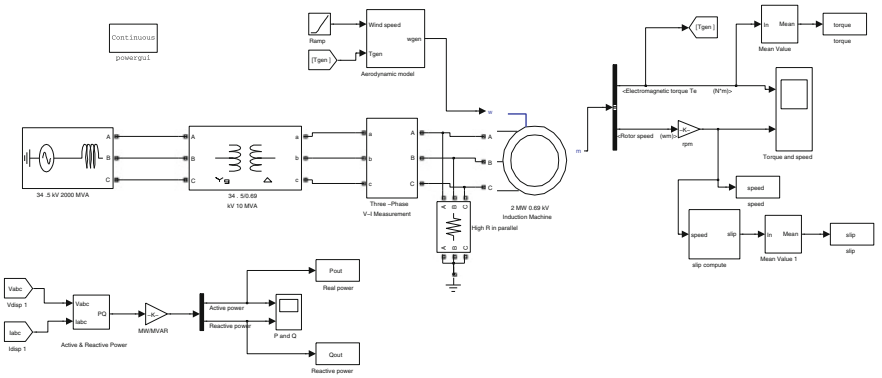


**Fig. 20** Fixed speed wind turbine model in SIMULINK

determined a subsystem block calculating the power available from the wind uses $C_p$ to determine the power extracted from the wind and thus, the aerodynamic torque of the rotor blades.

This input is then used in the two-mass model of the rotor shaft, gear train and generator shaft to solve the differential equations for generator speed ($\omega_{gen}$) and rotor speed ($\omega_{rot}$). The generator speed ($\omega_{gen}$) thus obtained is then fed to the built in asynchronous machine model in SIMULINK, with rotor circuit shorted and neutral grounded (squirrel cage mode). The electromagnetic torque ($T_{em}$) obtained from the machine model is then fed back to the two-mass model. Figure 20 shows the entire SIMULINK model of a fixed speed wind turbine, a multimeter measuring the stator voltage and currents is used, whose outputs are $V_{abc}$ and $I_{abc}$. The voltage and currents measured are used to determine the active and reactive power flowing out of the stator circuit of the machine.

The active and reactive power profile obtained from the SIMULINK model of the turbine are shown in Fig. 21. It can be seen that the active power peaks at 14 m/s, while there is no control over the reactive power generated. It remains negative, indicating that the machine constantly absorbs some reactive power from the grid. A typical fixed speed wind turbine power profile is obtained from the model, which is comparable to the PSCAD model described earlier in the previous section. After the wind speed crosses its rated value, the active power output of the machine drops to almost 1.2 MW.

A drop similar to the active power output of the machine can be seen in the torque profile too (see Fig. 22), at 14 m/s $T_{em}$ reaches a peak value of approx −12 kNm, as the wind speed increases beyond 14 m/s $T_{em}$ drops. A look at the speed profile of the machine, shows that it does not vary much during the entire wind speed sweep from 6 to 20 m/s it holds almost a constant value above 1,200 rpm and reaches a high of approx 1,205 rpm, when the wind speed reaches its rated value of 14 m/s. Overall, $\omega_{gen}$ variation with wind speed is very less. It can be observed from the torque slip characteristics of Fig. 23, that slip reaches a maximum value of −0.49 % at a maximum torque of approx −12,000 Nm. Thus, a peak torque (producing peak active

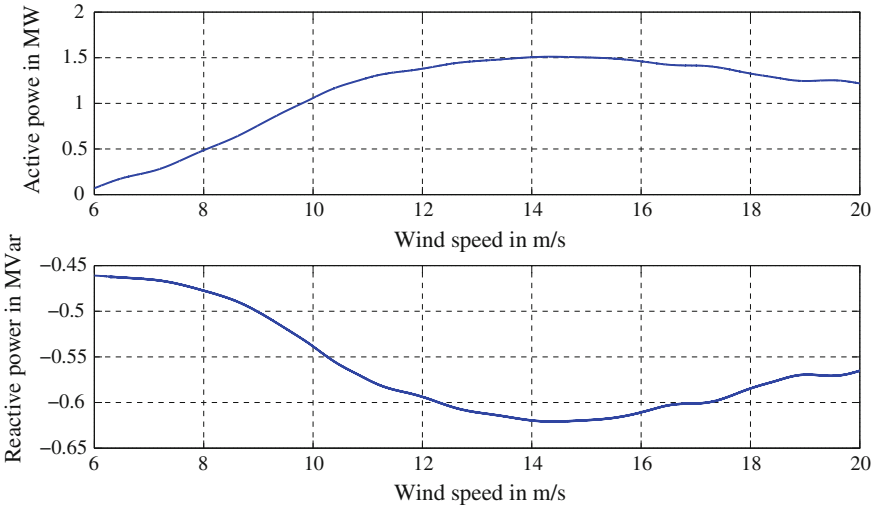


**Fig. 21** Active and reactive power profile for fixed speed wind turbine model in SIMULINK

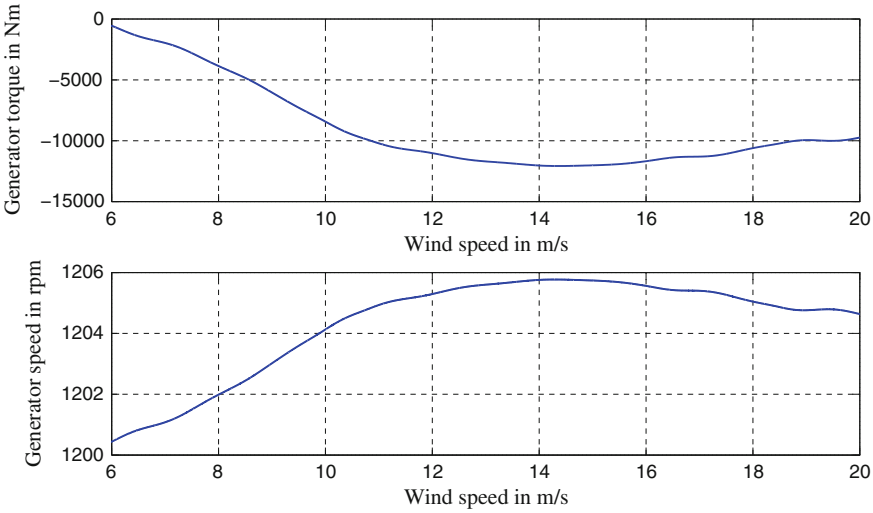


**Fig. 22** Generator torque and speed profile in SIMULINK

power) occurs at only one slip or speed value of the induction machine. The working and functional characteristics of a fixed speed wind turbine have been shown through models built on two different platforms. The results obtained are similar in many respects. The power profile, torque, speed and torque-slip characteristics obtained clearly show the stalling effect after rated wind speed. With the two models at hand, working of a fixed speed wind turbine and further grid integration of such a turbine can be studied in detail.

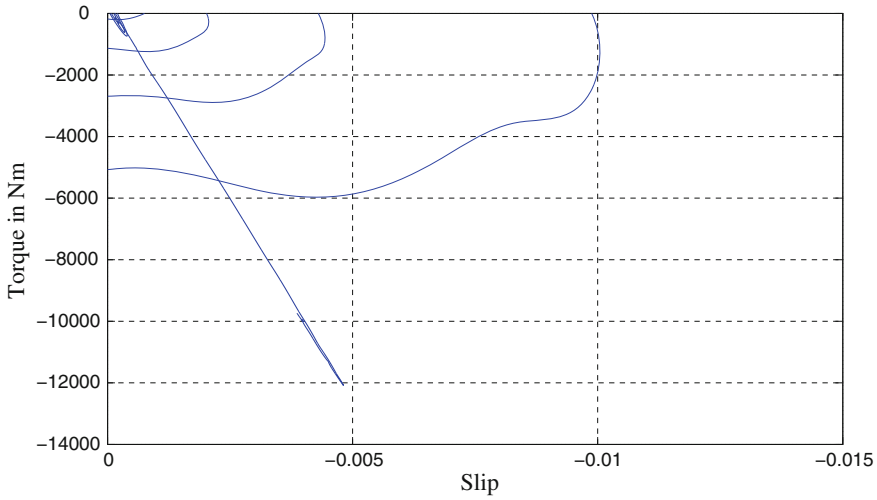


**Fig. 23** Torque slip characteristics of induction machine in SIMULINK

## *3.2 Variable Speed Wind Turbine*

As described in the previous section, for a fixed-speed wind turbine, there is no active control over the power output of the machine, once the rotor blade pitch angle is set. In variable-speed machines however, it is possible to control the output power using torque control. Various possible torque control methods exist to achieve constant power output above rated wind speed in variable-speed wind turbines. Two of these torque control methods are implemented in this chapter. These are:

- Aerodynamic torque control
- Generator torque control

Aerodynamic torque output from the rotor is determined by tip speed ratio and $C_p$, rotor geometry (blade pitch and aileron settings), wind speed, yaw error and rotor drag. Since, there is no control over the wind speed, other parameters have been used to control the aerodynamic torque. Any change in the tip speed ratio changes the rotor efficiency thus changing the rotor torque. A change in rotor geometry i.e. varying the rotor pitch angle results in a change in lift and drag forces thereby changing the torque output. Pitching the blade can regulate the torque output either by reducing the angle of attack or increasing it, as in case of stalling. Rotor blades for pitch-regulated wind turbines are designed to operate at maximum efficiency (maximum power production) for relatively high angles of attack (Fig. 24). At these high angles of attack, change in rotor blade position (typically moving the turbine into the stall region) is accomplished with more exact control, is faster and results in a quieter overall operation. The downside is that inducing

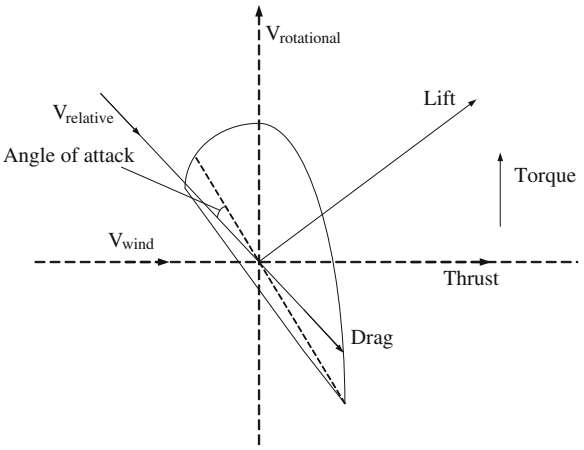


**Fig. 24** Blade geometry of horizontal axis wind turbine [12]

stalling from the very start results in unsteady loads, less accuracy in control, and greater thrust on the turbine due to unsteady nature of the stalled flow.

In case of generator torque control, torque of the generator can be either changed through the design characteristics or by the use of power converters. As demonstrated in the fixed speed wind turbine model, grid connected generators operate over a very small or no speed range and provide the required torque at or near synchronous speed, which depends on the type of machine (induction or synchronous). For a grid connected induction generator change in $\omega_{gen}$ is a small percentage of the synchronous speed, this results in low torque spikes and softer response. In contrast, for a synchronous generator any forced torque change results in an instantaneous compensating torque, which can result in higher torque and power oscillations.

An induction generator can very rapidly achieve any desired value of target torque by the use of a power converter. The converter determines the frequency, phase angle and value of the currents to be injected into the machine windings, this allows the machine to be set to any desired value of torque, thus controlling the power output of the generator.

### 3.2.1 Pitch Control

As explained above, aerodynamic torque control can be achieved by changing the rotor blade geometry (blade pitch angle $\beta$) for varying wind speeds. Pitch control is somewhat analogous to steam governor action in a synchronous machine, as both mechanisms control the mechanical input power to the generator. It can be visualized as fixed speed operation with an optimum pitch angle to produce maximum power at any wind speed above rated.

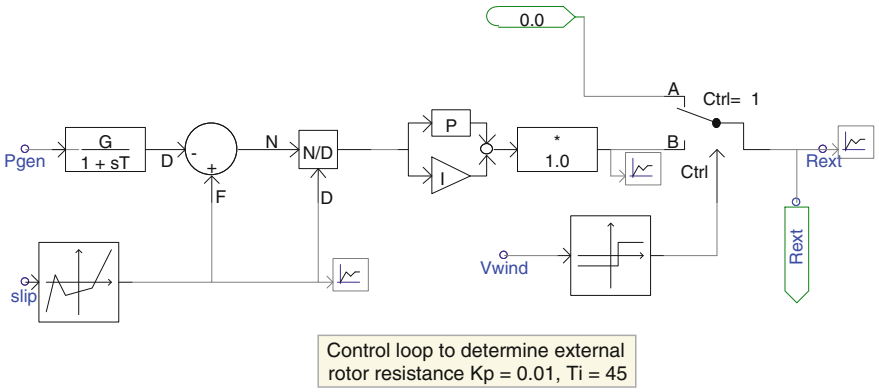


**Fig. 25** $R_{ext}$ estimation module in PSCAD using PI controller

### 3.2.2 Rotor Resistance Control

This section describes the simulation results of a variable speed wind turbine using PSCAD/EMTDC. PSCAD has been used to model and simulate the turbine. A built in machine model of a wound rotor induction machine is used to implement constant power and constant current strategy. The rotor pitch angle is set to −6.483° (rated pitch) to obtain a maximum power output of 1.5 MW at 14.2 m/s (rated wind speed). The wind turbine uses a 6-pole, 690 V, 1.8 MVA wound rotor induction machine as a generator.

**Constant power strategy to maintain constant power above rated wind speed**

Constant power strategy aims to maintain a constant power output of the WTGS above rated wind speed in the stall region. It was observed for the fixed speed WTGS, that output power falls as wind speed exceeds the rated value. With the use of PI controllers, rotor resistance of induction machine can be varied in such a manner, that active power output remains constant. To maintain constant active power output, reference value of active power is compared with actual power generated. The error signal is then fed to a PI controller. The output of the PI controller is the new value of single phase rotor resistance. Rotor resistance value thus calculated is equal for all three-phases. To obtain a rated slip of 2.25 % internal rotor resistance of 0.048 Ω is included in the rotor circuit. Figure 25 shows the PSCAD block diagram for the PI control implemented [14].

A rated slip of 2.25 % is obtained at 14.2 m/s and 1.5 MW output power. As the wind speed increases above the rated wind speed output power of the generator tends to fall. To maintain the output power constant calculated value of $R_{ext}$ is included in the rotor circuit, to increase the torque and thus the output power. To calculate the exact value of $R_{ext}$, actual generated power is compared with rated power (1.5 MW) and the corresponding error is converted into per unit (base as

**Table 1** Look-up table for PI controller tuning

| Parameter | Rise time | Settling time | Overshoot | Steady-state error |
|---|---|---|---|---|
| $K_p$ | Decrease | Small change | Increase | Decrease |
| $K_i$ | Increase | Increase | Increase | Eliminate |
| $K_d$ | Indefinite | Decrease | Decrease | None |

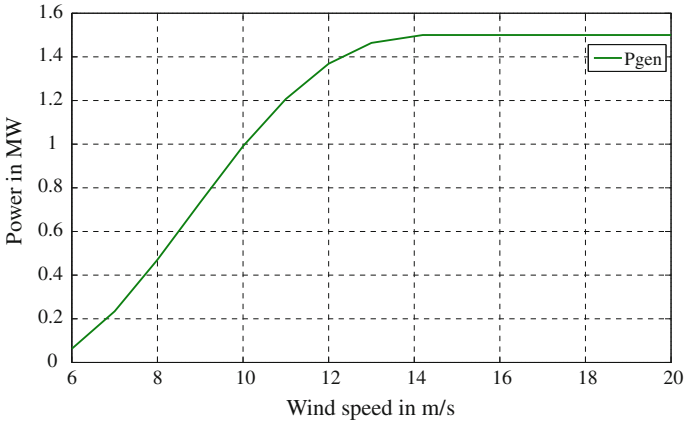


**Fig. 26** Wind power profile for a variable speed wind turbine using rotor resistance control

rated power) and error signal is fed to the PI controller. Once the output of the PI controller converges, $R_{ext}$ is obtained.

Ziegler Nichols tuning algorithm [15] was used to tune the PI controller. Tuning of the PI controller was done as follows:

1. Critical gain $K_c$ was found by setting a very high value of integral time constant $T_i = 10^6$ s. At critical gain $K_c = 0.026$ the output of the PI loop starts to oscillate sustainably, below $K_c$ the output just manages to converge and achieve a constant value. Further integral gain $K_i$ can be calculated using the formula shown. $K_i = \frac{1.2 \times K_c}{P_c} = 0.0226$ where $K_p = 0.45 \times K_c = 0.011$ and $P_c = 0.6$ s is the oscillation period of the PI controller output. $T_i = \frac{1}{K_i} = 45$ s.
2. Ziegler Nichols method is an iterative process. Using the values obtained above as initial values, further fine tuning of the controller was achieved following the Table 1. The table shows the effect of increasing or decreasing the proportional and integral gain $K_p$ and $K_i$ and was effectively used as guide in fine tuning the PI controller.

It is clear from the above Fig. 26 that power remains constant above rated speed of 14.2 m/s. The real power excursions with step changes in wind speed from 14.2 m/s (rated) to 15.2 m/s to 16.2 m/s are obtained using PSCAD model. Graph in Fig. 27 shows the real power excursions while the wind speed is changed in

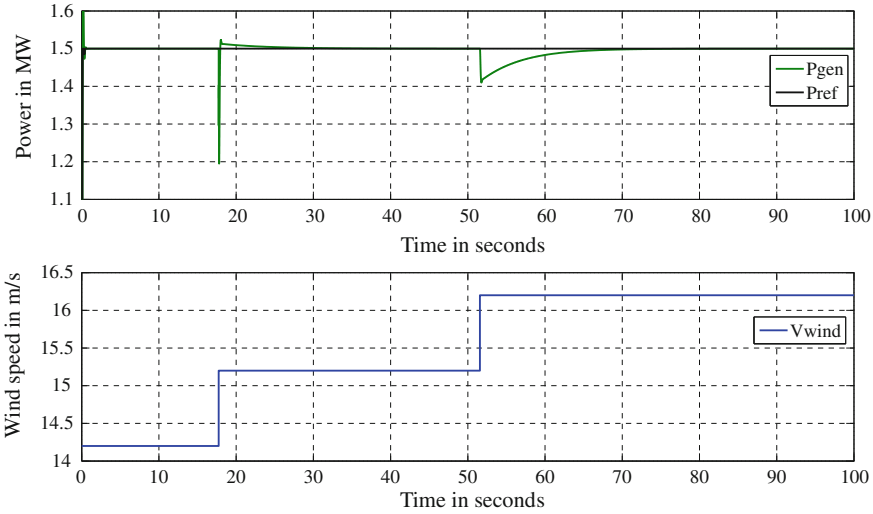


**Fig. 27** Power excursion: constant power strategy using PI control from 14.2 to 15.2 to 16.2 m/s

steps of 1 m/s, starting from 14.2 to 16.2 m/s. It can be seen that an undershoot for a wind speed change from 14.2 m/s(rated) to 15.2 m/s is quite large (1.5–1.2 MW). It can be attributed to the proportional gain and integral gain of the integrator. The PI controller when tuned for low undershoot and overshoot increases the settling time. It is also evident from the graph that the undershoot is very less (1.5–1.41 MW) for a step change from 15.2 to 16.2 m/s.

Power excursion for change in wind speed from 18 to 19 m/s (see Fig. 28) is more than that for 15.2–16.2 m/s, with a variation from 1.5 to 1.38 MW. It can also be seen that the undershoot increases over further step changes from 18 to 19 m/s (1.5–1.33 MW) and 19–20 m/s (1.5–1.26 MW) simultaneously the settling time goes down. Better results with reduced undershoots are demonstrated by the PID controller, at the cost of increased settling time, which seems like a reasonable trade-off.

It is observed that the power output of the generator is maintained constant at 1.5 MW above rated wind speed. As the slip increases, the frequency of rotor current $I_{rrms}$ increases.

**Torque slip characteristics in operating region**

The torque slip characteristics plotted in Fig. 29 shows a large variation of slip from 6 to 14.2 m/s. This increased slip variation is attributed to the internal rotor resistance $R_{int} = 0.048\ \Omega$ and can be changed to vary the rated slip from 2 to 2.5 %. As the slip variation is large over a range of increasing electromagnetic torque (negatively), the wind turbine can be controlled using PI controller to achieve a constant power output of 1.5 MW.

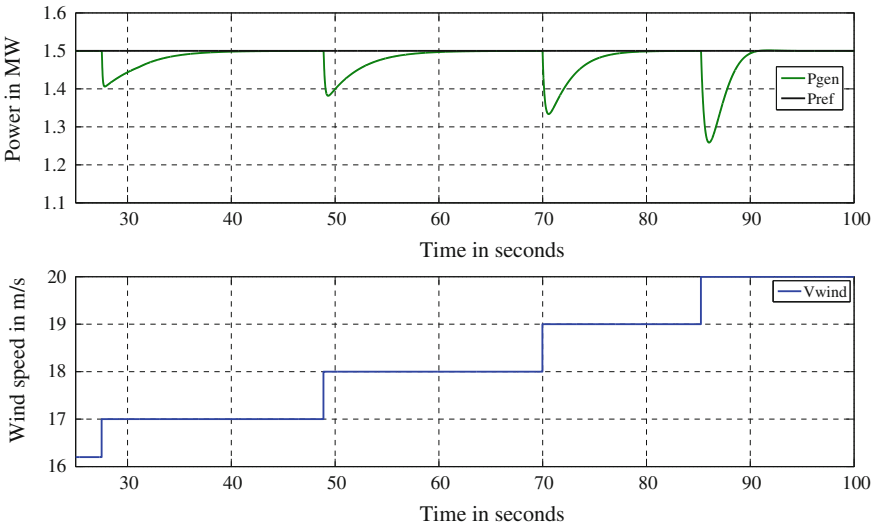


**Fig. 28** Power excursion: constant power strategy using PI control from 17 to 18 to 19 to 20 m/s

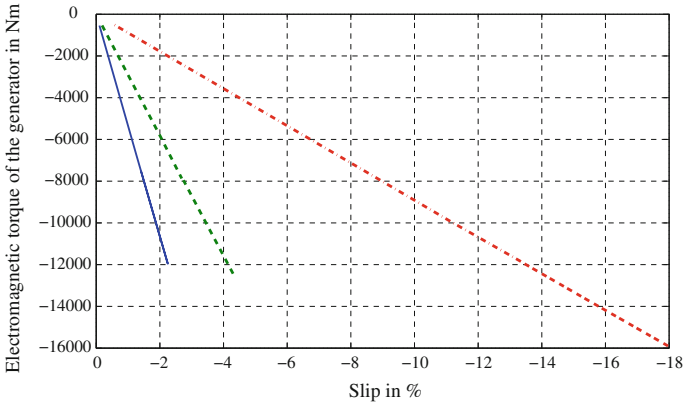


**Fig. 29** Torque slip characteristics with varying $R_{ext}$ at 8, 16 and 20 m/s wind speed

Another way of plotting the torque speed characteristics is by the use of electromagnetic torque formula as follows (Fig. 30),

$$\tau_e = \frac{3}{\omega_s} \cdot \frac{V_s^2}{\left(R_s + \frac{R_{rs}}{s}\right)^2 + (X_{ls} + X_{lrs})} \cdot \frac{R_{rs}}{s} \tag{49}$$

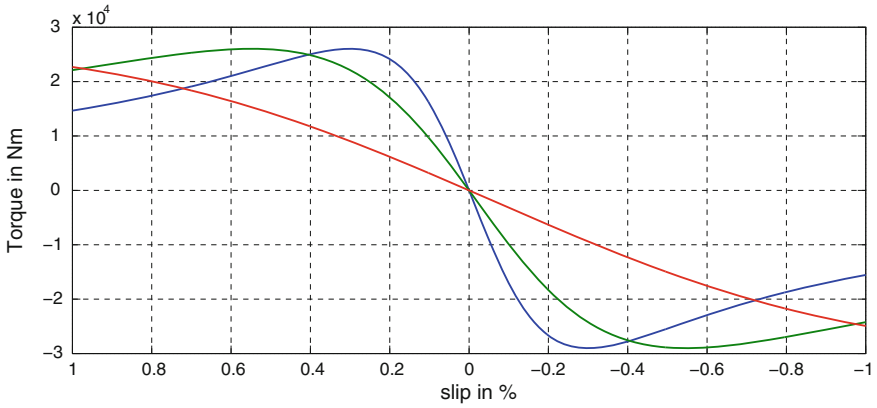


**Fig. 30** Complete torque slip characteristics with $R_{ext} = 0, 0.039, 0.22\ \Omega$ at 8, 16, 20 m/s wind speed respectively

where

| | |
|---|---|
| $\tau_e$ | Electromagnetic torque of the machine |
| $V_s$ | Generator terminal voltage |
| $\omega_s$ | synchronous speed |
| $R_s$ | stator resistance |
| $R_{rs}$ | Rotor resistance referred to the stator side |
| $X_{ls}$ | Stator leakage reactance |
| $X_{lrs}$ | Stator leakage reactance referred to the stator side |

To improve the transient response of the machine, for step changes in wind speed, a PID controller can also be used. PID controllers are tuned in a similar fashion as demonstrated for the PI controller.

A differentiator is included in the PI control loop to reduce the overshoot and settling time, with a flip side of increased system instability. Results obtained for the PID controller show improvements not only on reduced undershoot and no overshoot, but also highly accurate steady state value. As can be seen from the power excursion shown in Fig. 27 the undershoot goes as low as 1.2 MW and an overshoot of 1.52 MW. Opposed to this, the power excursion of the PID controller has improved undershoot of 1.38 MW and overshoot totally eliminated. This improvement can be attributed to the inclusion of the differentiator and reduced values of integrator time constant.

As visible from the Fig. 31, overshoot is almost eliminated and undershoot reduced with the use of PID controller. For a step change in wind speed from 14.2 to 15.2 m/s, the output falls till 1.38 MW and then tracks the rated value. Similarly, the undershoot for a change in wind speed from 15.2 to 16.2 m/s has been reduced to 1.41 MW.

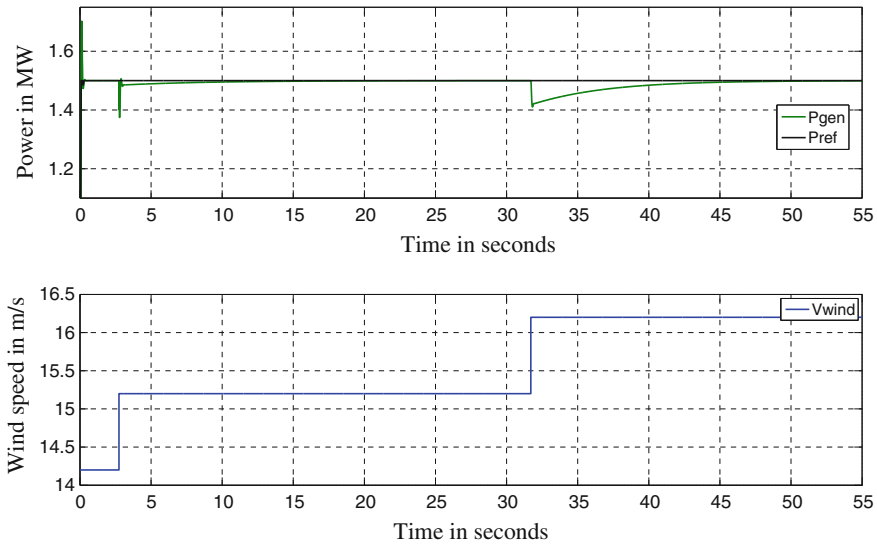


**Fig. 31** Power excursion: constant power strategy using PID control from 14.2 to 15.2 to 16.2 m/s

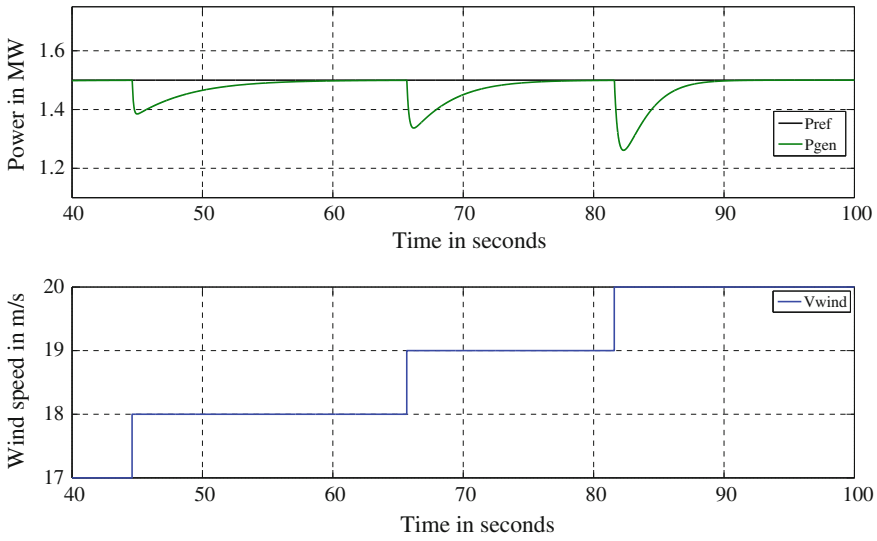


**Fig. 32** Power excursion: constant power strategy using PID control from 17 to 18 to 19 to 20 m/s

A similar power excursion profile can be seen in Fig. 32 for step change from 17 m/s to 18 m/s to 19 m/s to 20 m/s. The profile obtained is similar to that obtained with PI controller. Thus, a PID controller proves to be better in reducing the overshoots than the PI controller.

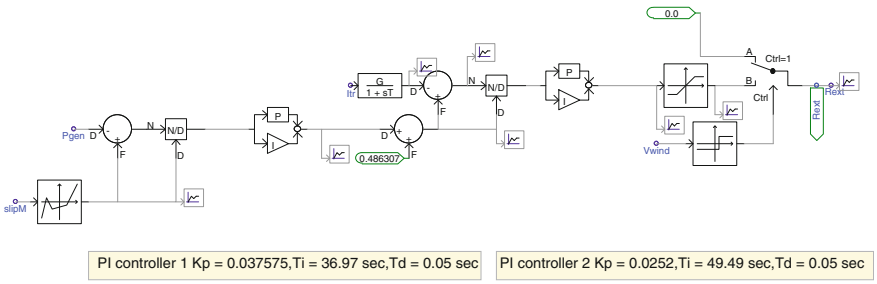


**Fig. 33** $R_{ext}$ estimation module in PSCAD using built-in PI controller

## Constant current strategy to maintain constant power above rated wind speed

Another method to implement variable speed wind turbine model is constant current technique. In this method rotor current is not allowed to fluctuate beyond a bandwidth. Initially, constant current was implemented using an error signal obtained from the $I_{rref} - I_{ract}$. Where, $I_{rref}$ is the rms value of rotor current at rated wind speed (with rated pitch) and $I_{ract}$ is the rms value of rotor current at any wind speed above rated. As we try to maintain the current in the rotor same as the rated value of rotor current, it was observed that the power output falls, above rated wind speed. The total variation in output power was 1.5–1.45 MW, for a range of wind speed from 14.2 to 20 m/s. Though the rotor current was maintained constant at rated value, the error current method did not provide a constant output power as desired for a variable speed wind turbine. This is due to the phase angle of the rotor current, which was not accounted, while maintaining constant current (only magnitude was considered).

To maintain output power constant, another error loop of $P_{ref} - P_{act}$ was added to the overall control loop calculating $R_{ext}$, where $P_{ref} = 1.5$ MW and $P_{act}$ is the actual power generated at any wind speed above rated. Error signal is then given to the PI controller. Output of the PI controller when added to the $I_{rated} = I_{ref}$. This $I_{ref}$ is then compared with $I_{act}$ and output fed to the PI controller. Output of the PI controller forms the $R_{ext}$ estimated. This method works, and is found to converge to constant power output eventually. Wind power profile remains the same as shown in Fig. 26), since the output power converges to 1.5 MW for all wind speeds above rated.

Initially a PI controller is used to implement constant current strategy. Tuning of the cascaded PI controllers in done using the same tuning algorithm as demonstrated for constant power strategy.

Value of the integral time constant set for PI loop 1 (Fig. 33) is not used as the final value. This is chiefly because, the final value of $T_i$ (integral time constant) also depends on proper tuning of PI loop 2 (Fig. 33).

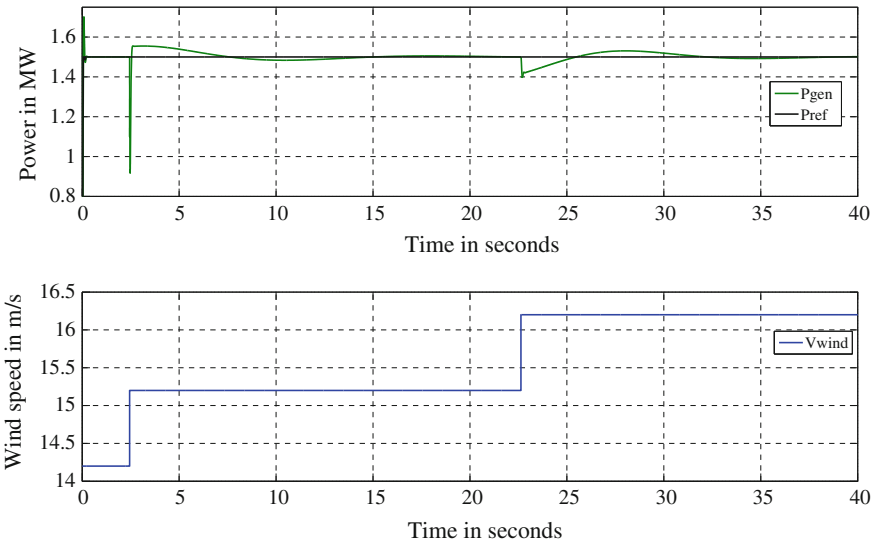


**Fig. 34** Power excursion: constant current strategy using PI control from 14.2 to 15.2 to 16.2 m/s

Power excursions for step change in wind speed from 14.2 to 15.2 to 16.2 m/s has been shown in Fig. 34. The settling time increases, with increased oscillations before the output settles.

The undershoot in this case is quite high 0.5 MW, while you can also see an overshoot till 1.9 MW. This is mainly because, there are two PI controllers, minimizing error in power output and then rotor current to obtain $R_{ext}$ so as to achieve constant power output of 1.5 MW. The power excursion for step change in wind speed from 15.2 to 6.2 m/s is far better, as the undershoot and overshoot is very less 1.4 and 1.55 MW respectively.

Though the power output converges after oscillating for some time, still the power excursions obtained using constant current strategy are worse as compared to constant power strategy. While obtaining a reference current for each wind speed, the rotor current oscillates a lot more as compared to the rotor current oscillations in constant power strategy.

Power excursion shown Fig. 35 is for step change in wind speed from 17 m/s to 18 m/s to 19 m/s to 20 m/s. With a step change in wind speed from 17 to 18 m/s, the output power oscillates from 1.38 to 1.57 MW, similarly larger oscillations can be seen for step wind speed change from 18 to 19 m/s and from 19 to 20 m/s. Even with increased oscillations, the power output converges and settles down to a constant value of 1.5 MW after some time.

Comparing the two methods used to achieve constant power, constant power strategy is clearly better than constant current. It is mainly due to reduced oscillations during power excursion for step changes in wind speed. Even the rotor current oscillations are less for constant power strategy. The phase angle of the

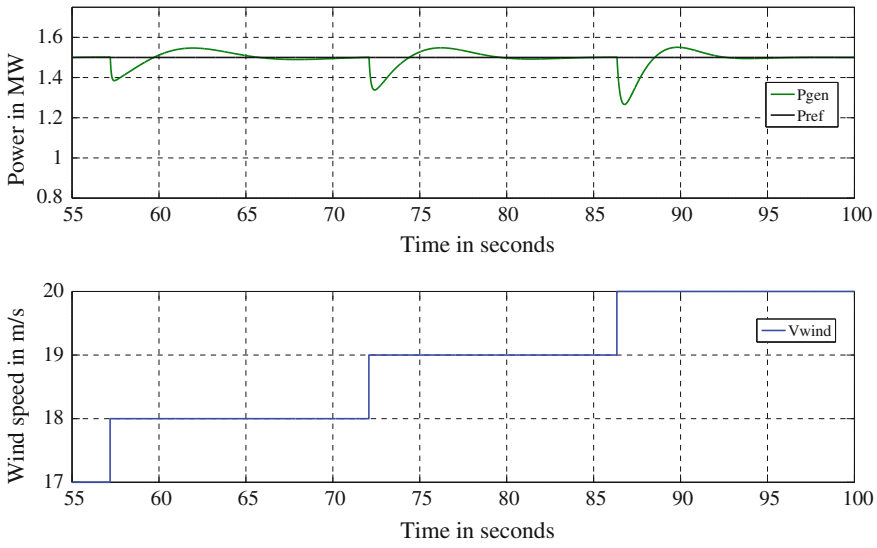


**Fig. 35** Power excursion: constant current strategy using PI control from 17 to 18 to 19 to 20 m/s

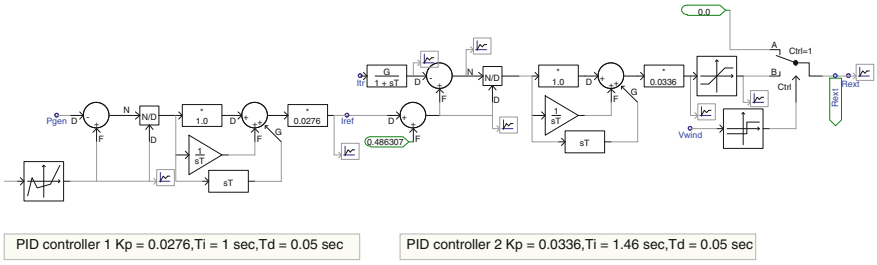


**Fig. 36** $R_{ext}$ estimation module in PSCAD using PID controller

rotor current has not been accounted for, while keeping the current magnitude constant. As we are considering only the current magnitude, results obtained using constant current strategy are not as accurate, as obtained using constant power strategy. To improve the accuracy of rotor resistance estimation, PID controllers are employed, it can be seen from the results obtained, that overshoots and undershoots have been reduced. Tuning of the PID controller is difficult as compared to the PI controller. Mostly because, inaccurate gain $K_d$ (differential gain) can make the system unstable (Fig. 36).

Value of the integral time constant set for PID loop 1 was not used as the final value. This is chiefly because, the final value of $T_i$ also depends on proper tuning of PID loop 2.

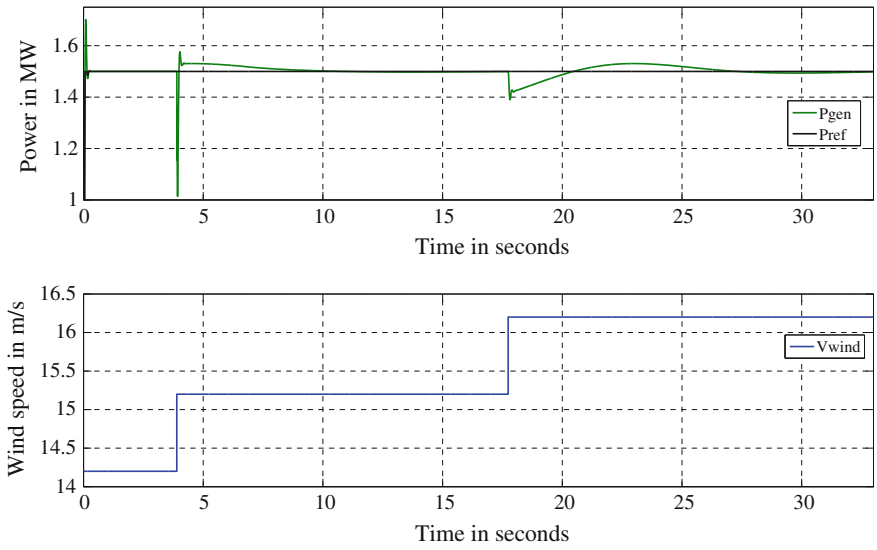


**Fig. 37** Power excursion: constant current strategy using PID control 14.2 to 15.2 to 16.2 m/s

Power excursions obtained for the PID controller are better than the PI controller, the undershoot has reduced and the output falls till 1.23 MW for step change in wind speed from 14.2 to 15.2 m/s. Similarly, the oscillation period and the settling time of the power output has also been reduced for the change in wind speeds shown in Fig. 37.

It is fair to conclude that the performance of self built PID controller is better than built in PI controller, even during wind speed change from 17 to 18 to 19 to 20 m/s there are less oscillations. Figure 34 can be compared with Fig. 37, while Fig. 35 can be compared with Fig. 38 to observe the difference, still the output fluctuates far more as compared to the constant power strategy implemented previously.

Constant power strategy and constant current strategy were successfully implemented with PI as well as PID controller for a variable speed wind turbine. The output power was maintained at 1.5 MW for any wind speed above rated wind speed of 14.2 m/s. If we compare the performance of PID controllers with PI controllers, it was observed that PID controllers, helped in reducing the undershoots, overshoots and oscillations in output power response. It was also observed that constant power strategy is more favorable for faster response with almost no oscillations as compared to constant current strategy.

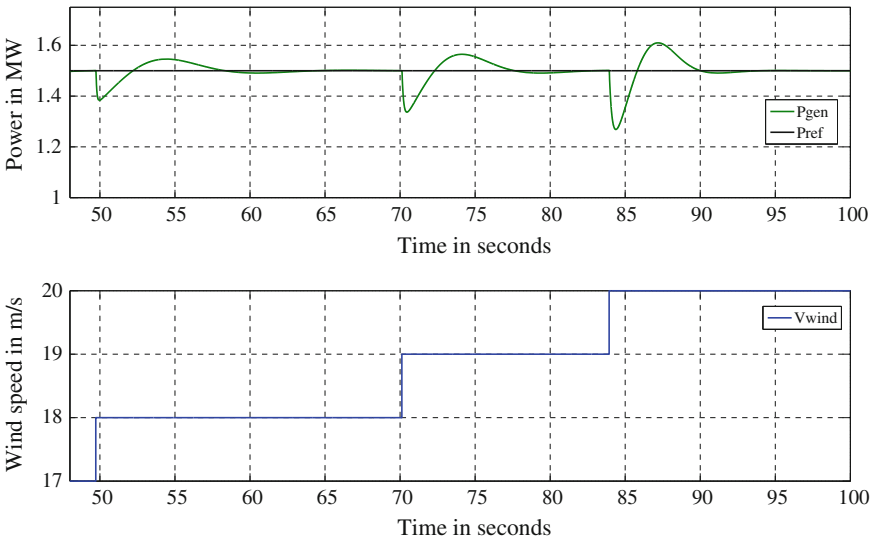


**Fig. 38** Power excursion: constant current strategy using PID control from 17 to 18 to 19 to 20 m/s

### 3.2.3 Hybrid Control

In the case of fixed speed wind turbine, the pitch angle ($\beta$) is set such that power output reduces with increase in wind speed beyond the rated speed. This is due to passive stalling above rated wind speed. The power extracted from the wind can be obtained from Eqs. (3)–(8). In case of rotor resistance control, external resistances are added to the rotor circuit to vary the slip or generator speed at which maximum generator torque is obtained. Since external resistance is implemented electronically, it responds fast to rises in wind speed [14]. However, due to the inclusion of the extra resistance, rotor thermal losses can be several hundreds of kW. A solution to this problem is adjusting the value of the blade pitch angle for the purpose of power control since $C_p$ is dependent on pitch angle as well. Since pitching rate is slow due to the high inertia of the rotor blades, rotor resistance can be included in the circuit only until the time the pitch is re-adjusted.

Figure 5 shows the $C_p$ versus $\lambda$ curves for different pitch angles. In low to medium wind speeds the pitch angle is controlled to allow the wind turbine to operate at its optimum condition (maximum $C_p$ condition). In high wind speed region, the pitch angle is increased to shed some of the available wind power. Figure 24 shows the blade geometry of a horizontal axis wind turbine. With increase in the pitch angle, the angle of attack decreases, decreasing the lift force resulting in reduced power output. Similarly, a reduction in the pitch angle increases the power output. Therefore, at low wind speeds the pitch angle is set low whereas at high speeds the angle is increased to relatively higher values.

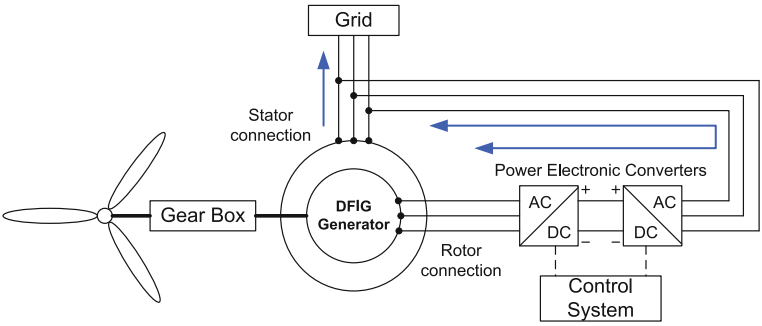


**Fig. 39** DFIG wind turbine schematic

## *3.3 Doubly Fed Induction Generator*

It has been already shown in the case of rotor resistance control that, variable wind speed turbines provide better optimization of output power produced by the rotor. In the case of rotor resistance control, changing the rotor resistance changes the slip and thus required torque is produced at varying wind speeds above rated wind speed. When induction machine operation is controlled by the use of power converters to achieve variable speed operation, it is observed that independent active and reactive power control can be achieved. The DFIG is a wound rotor induction generator in which the rotor windings are connected to the grid through power converters. Two VSIs are used for such a connection, linked using a DC link capacitor. With the use of a DFIG, it is possible to transfer power in both directions across the inverter-converter pair. This enables the generator to operate above and below the synchronous speed. Operating the machine over synchronous speed initiates a power flow from the rotor circuit to the grid, while operating the machine below synchronous speed (sub synchronous speed) initiates a power flow from the grid connected stator circuit to the rotor circuit. The amount of active and reactive power transferred to the grid and the machine slip are controlled by rotor current injection into the rotor circuit. For this purpose, reference frame theory is used to obtain *qd*0-axis rotor currents, which can independently control the active and reactive power output of the machine.

On comparison with traditional induction generator, DFIG configuration has many advantages:

- Provides the ability to achieve independent active and reactive power control.
- Supports grid voltage by controlling the reactive power produced or absorbed, which helps maintain a stable grid voltage.

A schematic representation of a DFIG wind turbine system is shown in Fig. 39. In DFIG turbines, the induction generator is a wound-rotor induction machine. Because only part of the real power output flows through the rotor circuit, the power rating of the converter need only be about 20–30 % of the rated turbine

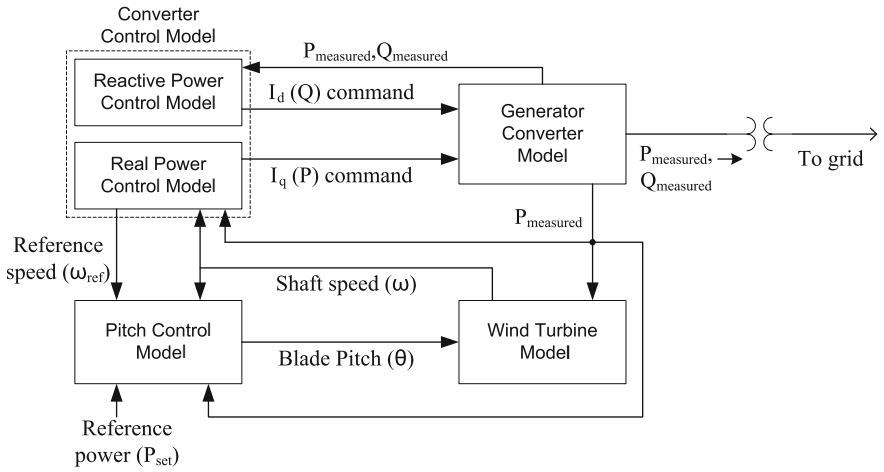


**Fig. 40** DFIG model structure

output. A control system is employed to regulate currents in the rotor to extract the maximum possible power from the wind.

The reference wind power plant has a nameplate rating of 204 MW and consists of 136 DFIG wind turbines, each rated at 1.5 MW. Any other WPP can be modeled by changing model parameters. It is connected to the transmission system at 138 kV. The collector system employs 34.5 kV feeders and is adjacent to the transmission station. The wind power plant is equipped with a voltage regulator that controls voltage at the transmission station, relying on the reactive power capability of the WTGs only. There is no additional reactive compensation within the wind power plant.

The subsystems of the developed general wind power plant model are modeled after the subsystems of a typical real-world DFIG turbine. These functionalities include the independent control of real and reactive power and the control of generator speed and blade pitch angles. They are summarized as follows:

- Generator/converter model
- Converter control model
- Wind turbine mechanical model
- Pitch control model
- Collector system

Figure 40 shows the connection of these subsystems and the signals they exchange.

The model is meant to represent the aggregate terminal behavior of the typical WTGS in the wind power plant. In an actual wind power plant, a local grid collects the output from the wind turbines into a single point of connection on the grid. As a wind power plant is usually made up of several identical machines, it is a reasonable approximation to parallel all the turbines into a single equivalent large

turbine behind a single equivalent impedance. The power rating of the single equivalent wind turbine is equal to the combined rated power ratings of all wind turbines on the farm. The single machine equivalent also assumes that all the machines generate the same power output at the same time. This assumes that the geographic area occupied by the wind farm is small enough that the wind profile over it is uniform.

A point to be noted is that the electrical dynamic performance of DFIGs at fundamental frequency is dominated by the converter. The combined electrical behavior of the generator and converter in the DFIG is largely like that of a current-regulated voltage source inverter, which may be simplified for modeling purposes as being equivalent to a regulated current source. Therefore, the generator and converter can be combined and modeled as a single current source. This current source is controlled using flux-vector control to obtain the desired real and reactive power flows.

Flux-vector control allows the decoupled control of real and reactive power. For decoupled control over real and reactive power output a controller based on flux-vector control was modeled. As mentioned before, wound rotor induction machines are used in DFIG wind turbines. In the stationary *abc* reference frame, the relationships between the voltages, currents and flux linkages of each phase for a machine of this type are time variant. Analysis in this reference frame is cumbersome, so time variant quantities are made time invariant by transforming them into an appropriate rotating reference frame, i.e. the rotating *qd*0 reference frame. The currents flowing in the stator are assumed to be balanced. These currents produce a resultant stator magnetic field which has a constant magnitude and is rotating at synchronous speed. Since the angular speeds of the stator magnetic field and the *qd*0 rotating frame are identical, the vector of the stator magnetic field is fixed with respect to the *q*- and *d*-axes of the *qd*0 rotating frame. The *d*-axis of the reference frame is oriented in such a way that it aligns with the vector of the stator magnetic field. The real and reactive power can be controlled by adjusting the stator *q*- and *d*-axis current. The stator *q*- and *d*-axis currents can be controlled by adjusting the rotor *q*- and *d*-axis currents. The stator real and reactive power can thus be written as:

$$P_s = k_{ps} \cdot i'_{qr} \tag{50}$$

$$Q_s = -k_{qs1} + k_{qs2} \cdot i'_{qr} \tag{51}$$

where $k_{ps}$, $k_{qs1}$, and $k_{qs2}$ are the respective constants for the stator real and reactive power. Equations 50 and 51 clearly show that the stator real and reactive power can be controlled by the rotor *q*- and *d*-axis currents independently. In both the positive-sequence model and the three-phase model, the reference *q*- and *d*-axis currents are generated by the converter control block, as shown in Fig. 40. In the three-phase model, these *q*- and *d*-axis currents are converted back to three-phase currents using the inverse Park transform [13] prior to injection into the collector

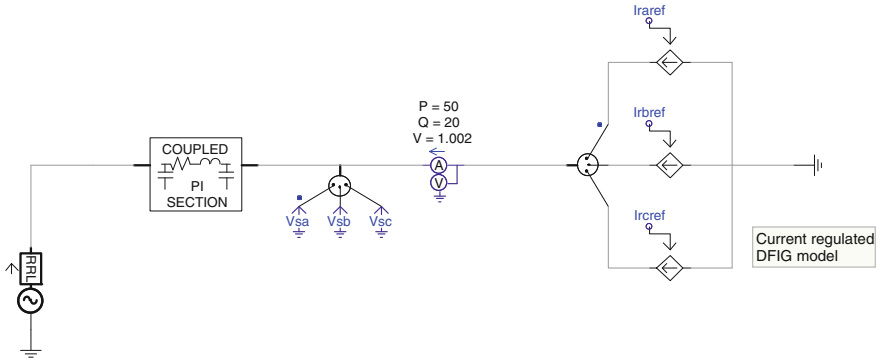


**Fig. 41** DFIG model in PSCAD

system. The other subsystems, namely, the converter control model, wind turbine mechanical model, and pitch control model have been modeled in the same manner as in [22].

### 3.3.1 PSCAD Model

This section describes the simulation results for a current regulated representation of doubly fed induction generator (DFIG) using PSCAD/EMTDC (Fig. 41). The real and reactive power of a wind turbine generator can be independently controlled using a doubly-fed induction generator. A current regulated representation of DFIG is modeled and principle of flux vector control applied to show independent P and Q control. Steps involved in developing the model and implementing vector control, along with results obtained have been shown.

1. Perform Clarke Transform (abc-$\alpha\beta$): Stator voltage $V_{sa}$, $V_{sb}$, $V_{sb}$ are converted from three-axis (abc) quantities to two-axis quantities ($\alpha\beta$) $V_\alpha$ and $V_\beta$ by performing Clarke transform. Obtained two-axis voltages are integrated to obtain corresponding flux values ($\lambda_\alpha$, $\lambda_\beta$). Instantaneous value of stator flux $\lambda_s$, its magnitude and angular position are determined. A sample run is performed for $P_{genref} = 50$ MW, $Q_{genref} = 20$ MVAR to obtain a sample value of instantaneous stator flux magnitude and angular position. $\lambda_{total} = |\lambda_s| =$ constant, whereas the angular position being an instantaneous value it keeps on varying during the simulation run time. Thus, we obtain a constant magnitude rotating vector $\lambda_s$ (Fig. 42).
2. Perform Park Transform ($\alpha\beta$ − dq0): A synchronously rotating frame $qd0$ at synchronous speed $\omega_s$ is constructed and stator flux aligned along d axis to obtain $|\lambda_d| = |\lambda_s| =$ constant, and $|\lambda_q| = 0$.

Stator d and q voltages are also computed and found to be $V_d = 0$ kV, $V_q = 28.2107$ kV (Fig. 43).

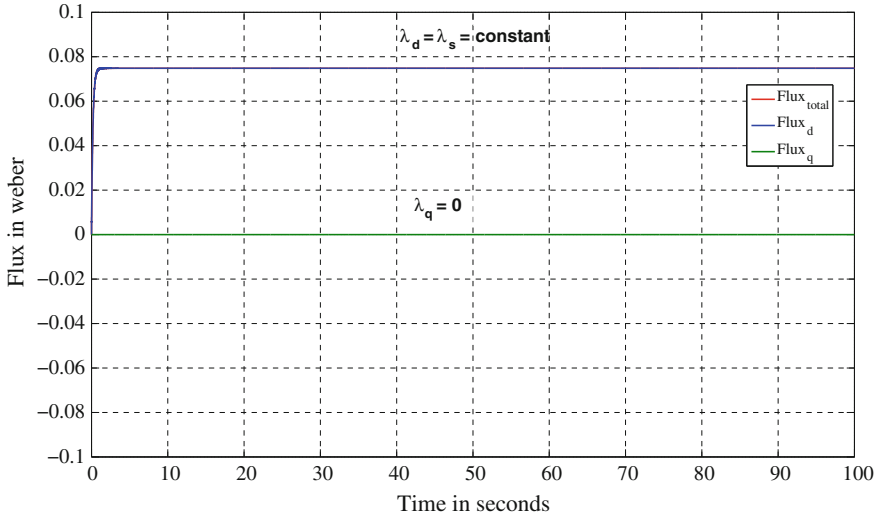


**Fig. 42** $|\lambda_d| = |\lambda_s| =$ constant and $|\lambda_q| = 0$

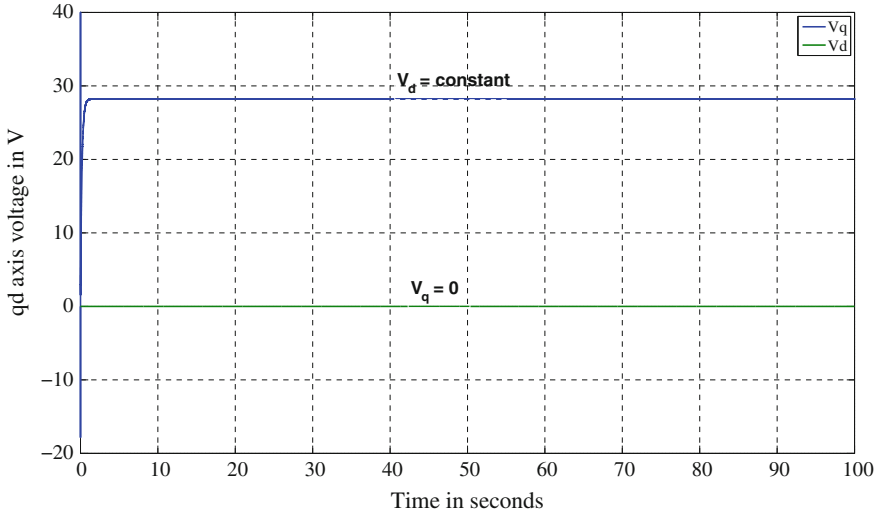


**Fig. 43** Voltage along d-q axis

3. Assuming that available wind power is sufficient to generate the desired level of apparent power, reference values for real and reactive power are set to sample values $P_{genref} = 50$ MW, $Q_{genref} = 20$ MVAR. Value of reference currents to be given to the regulated current source is found out, by comparing the generated power with reference power values.

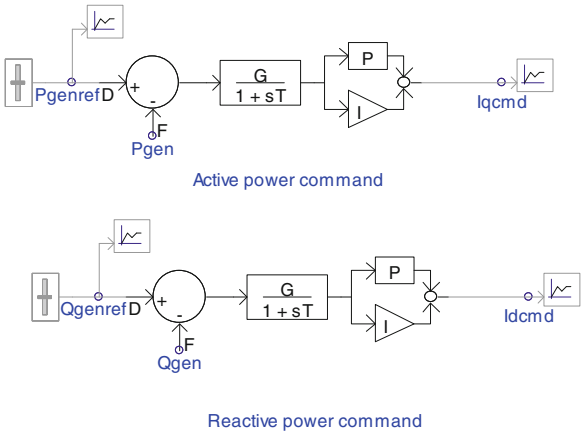


**Fig. 44** Computing reference currents $I_d$ and $I_q$

4. The reference or command currents thus obtained along *dq-axis* ($I_d$, $I_q$) can be converted into currents along *αβ-axis* ($I_\alpha$, $I_\beta$) through inverse park transform and eventually into currents along *abc-axis* ($I_{raref}$, $I_{rbref}$, $I_{rcref}$) using inverse Clarke transform. It can be shown through real and reactive power equations developed in vector control theory, that the active power from the generator is controlled by $I_q$, while reactive power by $I_d$ (Fig. 44).
5. The output is measured for different values of desired power and power generated is found to track accurately the desired value. Further, to establish decoupled or independent control of real and reactive power, $Q_{gen\text{-}ref} = 20$ MVAR is kept constant and $P_{genref} = 50$–$400$ MW with steps of 50 MW and corresponding $P_{gen}$ and $Q_{gen}$ values are registered. It is clearly seen from Fig. 46 that with step change of 50 MW in real power, reactive power remains constant as we increase the desired real power from 50 to 400 MW. There are small overshoots during transient period, but the output settles really fast. Thus, it is demonstrated that, reactive power change is independent of real power demand. It can be satisfactorily established from Fig. 46 that step changes of 20 MVAR in reactive power have no change in the real power output of the DFIG. Thus, Fig. 46 confirm independent P and Q control (Fig. 45).

### 3.3.2 MATLAB/SIMULINK Model

Modeling in SIMULINK involved developing the model in parts:

1. Developing the abc-αβ-qd0 and inverse transformation blocks.
2. Using controlled current sources to inject reference currents at stator or grid frequency.

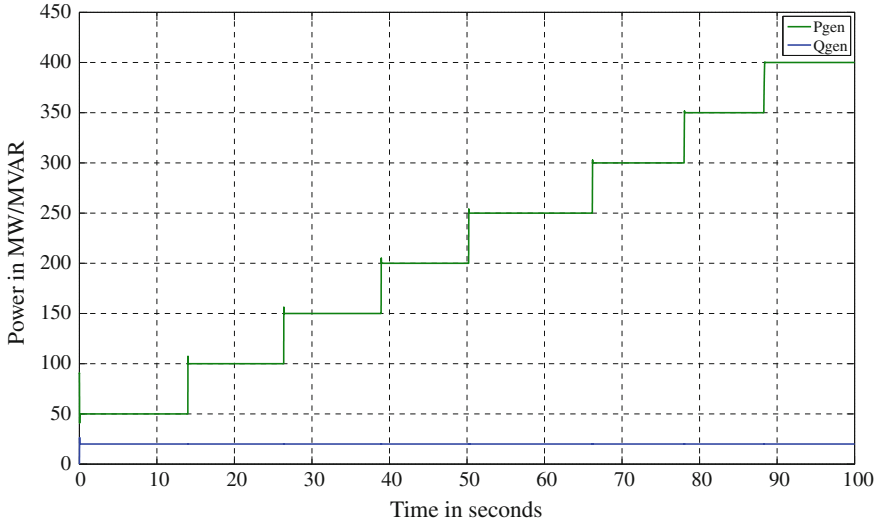


**Fig. 45** $P_{genref} = P_{gen} = 50$–$400$ MW in steps of 50 MW, $Q_{genref} = Q_{gen} = 20$ MVAR

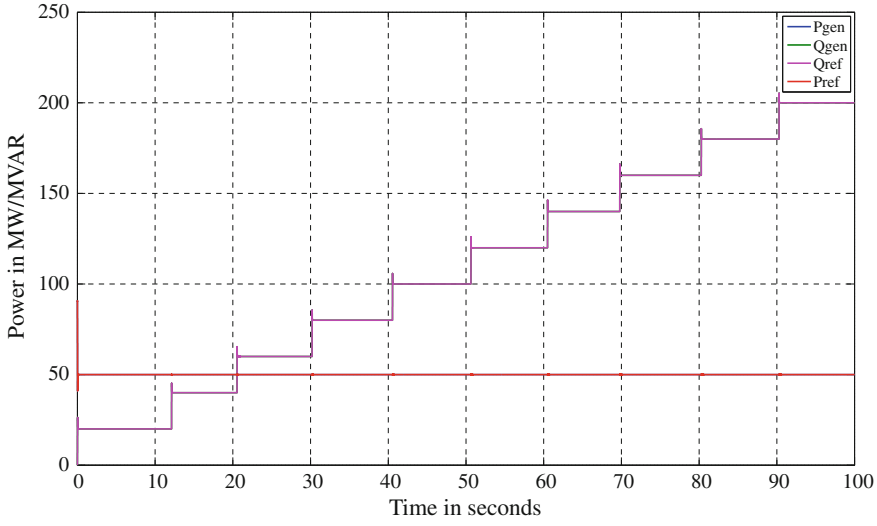


**Fig. 46** $Q_{genref} = Q_{gen} = 50$–$400$ MW in steps of 50 MW, $P_{genref} = P_{gen} = 50$ MW

3. Tuning the PI controllers to compute $I_d$ and $I_q$ command currents by comparing $P_{ref}$ and $Q_{ref}$ with $P_{gen}$ and $Q_{gen}$ respectively.
4. Demonstrate successful power tracking and decoupled control of P and Q.

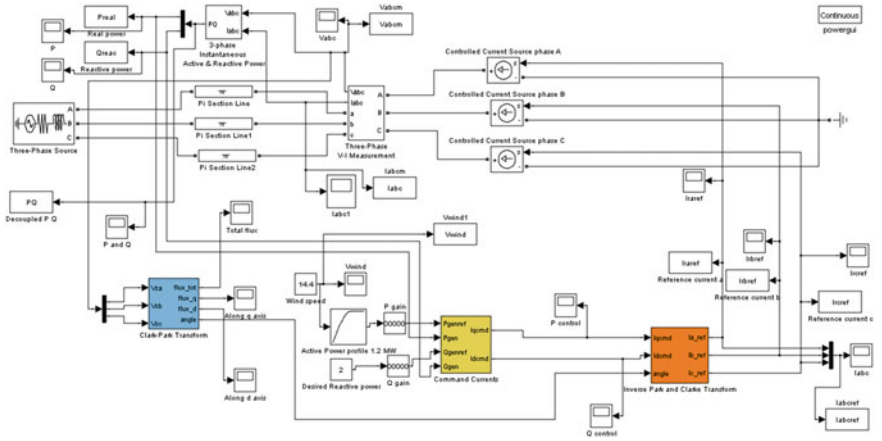

**Fig. 47** Block diagram of DFIG model in SIMULINK

5. Develop and use a look up table approach to compute reference P and reference Q for a 1.8 MVA machine, 1.5 MW rated active power at rated wind speed of 14.2 m/s.

Stator voltage in the *abc* frame and at the grid frequency of 60 Hz and are measured and transformed to $\alpha\beta$ stationary frame to obtain two axis voltages $V_\alpha$ and $V_\beta$ from $V_{abc}$. Further, the voltage signals are integrated to obtain the flux along $\alpha\beta$ axis. A rotating qd0 frame is then constructed and q-axis aligned with stator field. The newly created qd0 frame rotates at grid frequency or stator frequency. With *qd*0 frame constructed and sample input values for voltage showing proper alignment of q-axis with stator field, the next part of modeling the DFIG includes, using current controlled sources (representing induction machine) to inject currents into the grid.

As such controlled sources are available in SIMULINK. Using the current source blocks available in SIMULINK and an entire block modeling a three phase voltage source as grid and *pi* sections representing transmission lines are used. Given below is the specification for grid parameters and transmission line parameters used initially (Figs. 47 and 48).

Grid voltage = Vs = 34.5 kV
Grid frequency = fs = 60 Hz
MVA base = 100
X/R ratio = 10

Transmission line parameters for a three phase line

R = 0.2568 Ω/km
L = $2 \times 10^{-3}$ H/km
C = $8.6 \times 10^{-9}$ F/km
Length of the line = 100 km

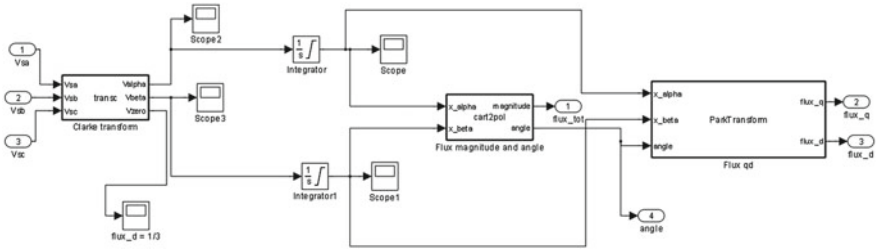


**Fig. 48** Block diagram for $abc - \alpha\beta - qd0$ tranformation

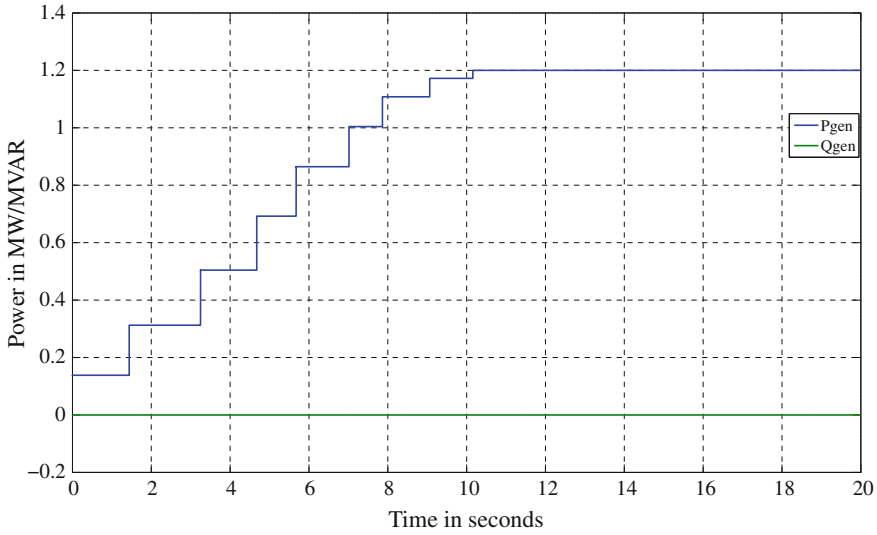


**Fig. 49** Active power excursion

3-$\phi$ multi-meter available in SIMULINK was used to measure $I_{abc}$ and $V_{abc}$. An in built complex power measurement unit is used to measure active and reactive power. PI controller is $I_{qcmd}$ and $I_{dcmd}$ command currents, by comparing the actual values of active power and reactive power with the reference values respectively. Tuning of the PI controllers is performed using Ziegler Nichols method as explained in Sect. 3.2.2.

Once the PI controllers are tuned, $I_{qcmd}$ and $I_{dcmd}$ command currents are transformed using Inverse Park and Inverse Clarke transform to obtain $I_{aref}$, $I_{bref}$, $I_{cref}$ reference currents for the controlled current sources. As shown in Fig. 49 P and Q can be controlled independently to achieve "Power factor correction" or "voltage regulation", i.e. the wind turbine can produce reactive power to maintain the voltage constant or keep the reactive power output to 0 MVAR. To demonstrate

**Table 2** Power tracking

| Wind speed (m/s) | Active power P (MW) |
|---|---|
| 6 | 0.138232 |
| 7 | 0.312485 |
| 8 | 0.504339 |
| 9 | 0.692401 |
| 10 | 0.864456 |
| 11 | 1.00413 |
| 12 | 1.10796 |
| 13 | 1.17216 |
| 14.4 (rated) | 1.2 |
| 15 | 1.2 |
| 16 | 1.2 |
| 17 | 1.2 |
| 18 | 1.2 |
| 19 | 1.2 |
| 20 | 1.2 |

active power tracking for a given wind turbine Table 2 is used to plot the power profile. Table 2 shows the amount of active power to be generated for a particular wind speed. Wind turbine used to obtain the power profile shown in the table below is rated at 14.4 m/s at $+0.165^{\circ}$ pitch angle and rated active power for the generator is 1.2 MW (machine rated for 1.8 MVA). The maximum rated power obtained for the given $C_p$ versus $\lambda_r$ a characteristic is 1.2 MW (Fig. 50).

## *3.4 DFIG Model Validation*

The aim of the validation process is to demonstrate and prove that the DFIG does indeed behave like a real-world DFIG wind power plant, especially during fault conditions. A fault case is used to test the time-domain model. Actual data for three-phase voltages and currents (at the bus where the collector system is connected to the grid) has been provided in the data from the real-world wind power plant. Also, the reactive power demand was set to zero, but the real power (dependent on the wind speed) was set to a differing constant value. The validation procedure for the three-phase model is detailed in Fig. 51.

### 3.4.1 Calculation of Real and Reactive Power in MATLAB Script

The following calculations are carried out in the MATLAB script mentioned in Fig. 51. The voltage $[v_{abcs}]$ and current $[i_{abcs}]$ extracted from the time-domain model are converted from values on the stationary *abc* frame to equivalent values on the rotating *qd*0 reference frame. This is done using the Park Transform shown below:

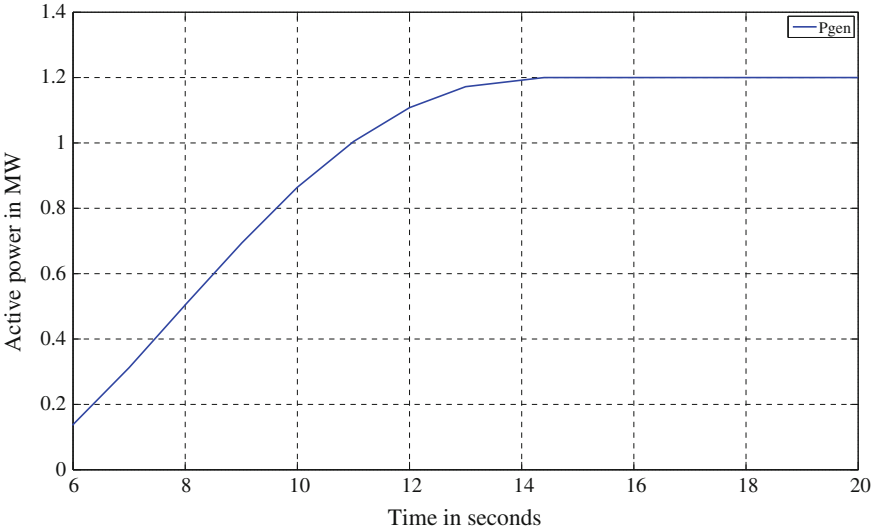


**Fig. 50** Wind active power profile for the DFIG

$$[T_{qd0}] = \frac{2}{3}\begin{bmatrix} cos\theta_q & cos(\theta_q - \frac{2\pi}{3}) & cos(\theta_q + \frac{2\pi}{3}) \\ sin\theta_q & sin(\theta_q - \frac{2\pi}{3}) & sin(\theta_q + \frac{2\pi}{3}) \\ \frac{1}{2} & \frac{1}{2} & \frac{1}{2} \end{bmatrix} \tag{52}$$

The following transformation equations can then be used [13] to convert phase voltage and current quantities into the $qd0$ domain.

$$[v_{qd0s}] = [T_{qd0}] \cdot [v_{abcs}] \tag{53}$$

$$[i_{qd0s}] = [T_{qd0}] \cdot [i_{abcs}] \tag{54}$$

It is possible to align the $d$- and $q$-axis quantities in such a manner that the $d$-axis voltage is zero. The calculation of real and reactive power can then be performed using the following equations (where subscript $s$ signifies stator quantities):

$$P_s = \frac{3}{2}(v_{qs} \cdot i_{qs}) \tag{55}$$

$$Q_s = -\frac{3}{2}(v_{qs} \cdot i_{ds}) \tag{56}$$

### 3.4.2 Validation Based on Pre-fault Data

The first stage of the validation was to calculate the pre-fault real and reactive power for each phase in the phasor-domain using one cycle of pre-fault voltage

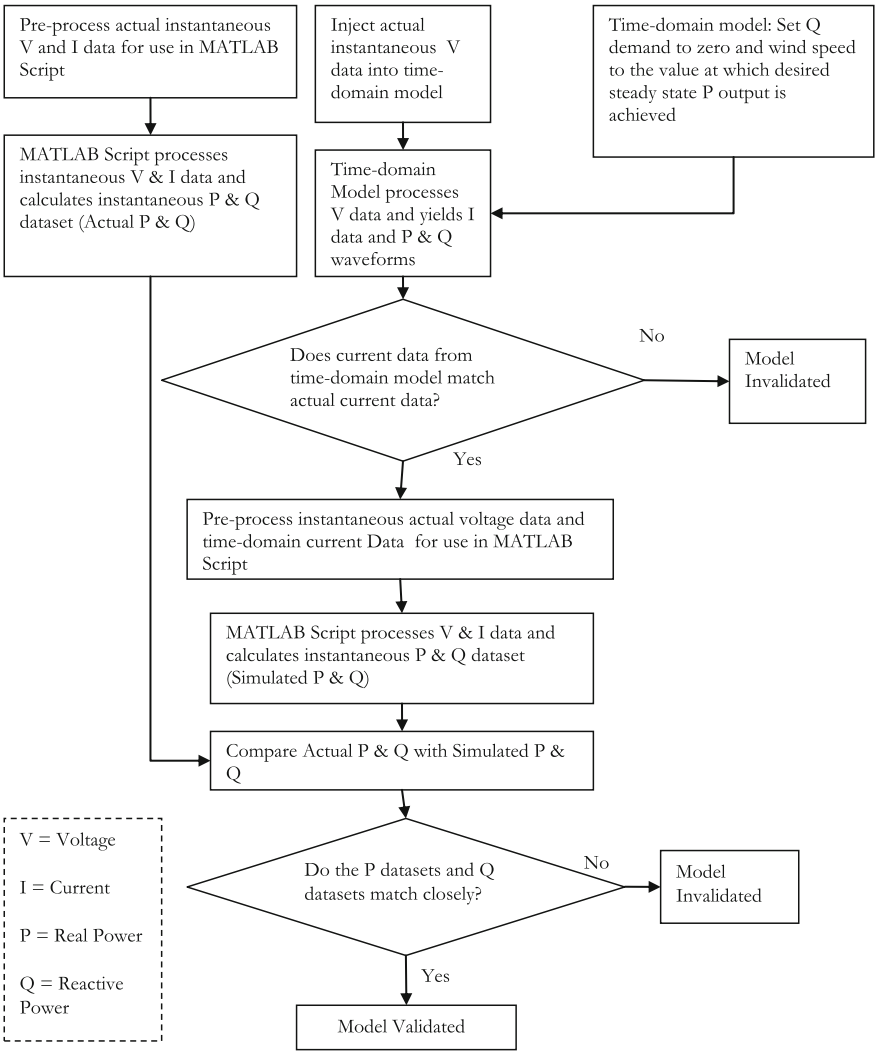


**Fig. 51** Validation procedure flowchart

and current from the actual fault data. Since the system is in steady state and the voltages are balanced, one cycle of the steady state voltage and current for phase A is adequate for calculations. The sign convention used is to consider real and reactive power flowing out of the wind plant model to be positive and into the wind plant model to be negative. Once the real and reactive powers in the phasor-domain were obtained, the next stage of the validation was to use the script to compare the actual data and time-domain model output data. The real power and reactive power values generated from the actual data and the data extracted from

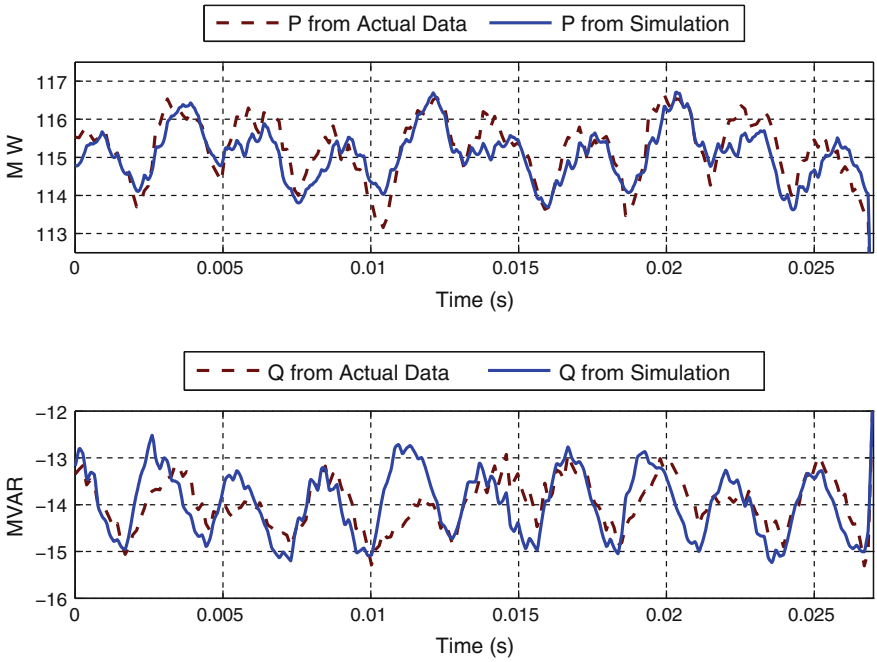


**Fig. 52** Steady-state: reactive power comparison: actual versus time domain model

the time-domain model match closely. They also match with the values obtained from phasor-domain calculations (see Fig. 52).

The calculations in phasor-domain for phase A were as follows:

$V_{rms} = 80.74$ kV
$I_{rms} = 559.38$ kA
$(V_{ph} - I_{ph}) = -8.96°$
$P_{1\phi} = V_{rms} \bullet I_{rms} \bullet \cos(V_{ph} - I_{ph}) = 44.61$ MW
$Q_{1\phi} = V_{rms} \bullet I_{rms} \bullet \sin(V_{ph} - I_{ph}) = -7.03$ MVAR
$P_{3\phi} = 3 \bullet (44.61)$ MW $= 133.84$ MW
$Q_{3\phi} = 3.(-7.03)$ MVAR $= -21.10$ MVAR

### 3.4.3 Fault-Time Validation

To evaluate the performance of the time-domain model during fault conditions, the validation process described earlier is used. The real and reactive power datasets 1 and 2 were generated and plotted together in order to compare the closeness of the match (See Fig. 53). The results show a close match, both in magnitude and phase. The wind power plant model provides a good approximation of the behavior of an actual wind plant under steady state and fault conditions. There are

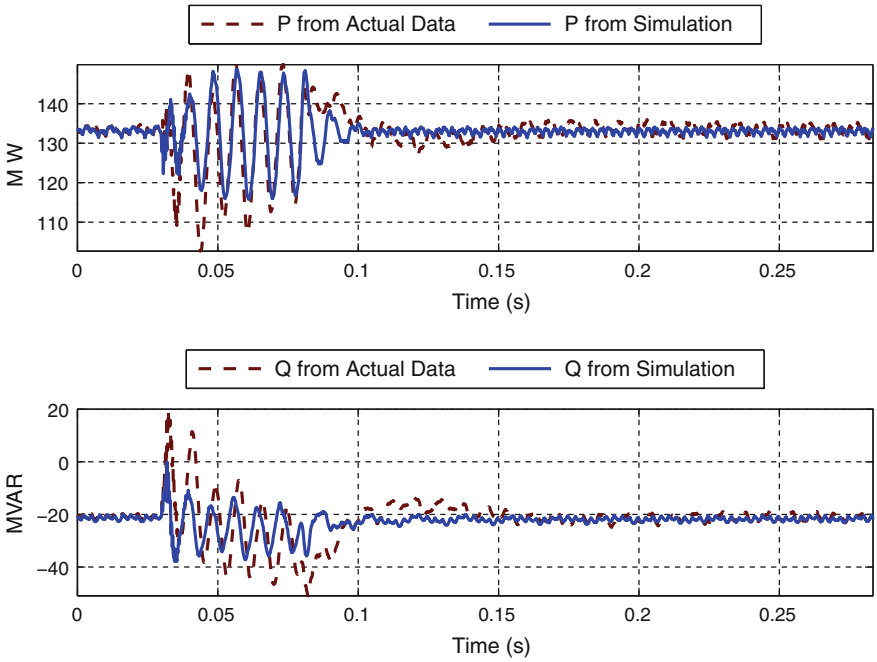


**Fig. 53** Comparison between actual and simulation-based real power and reactive power during fault condition

some small discrepancies between the real and reactive power plots obtained from the actual real and reactive power dataset (actual P and Q) and simulated real and reactive power dataset (simulated P and Q). These discrepancies may be due to the simplifications made to the time-domain model in order to preserve its general nature, since the induction generator and the power electronic converter are not explicitly modeled.

The three-phase WPP model has been comprehensively validated using instantaneous voltage, current, real power and reactive power fault data. A method to calculate WPP real and reactive power output from available voltage and current data at the POI has been presented. The results show that, as expected, the three-phase model is better able to reproduce the fault dynamics observed in the actual case.

## 4 Conclusion

This chapter presents a direct-connect fixed-speed wind turbine model, a variable-speed rotor-resistance control wind turbine model, and a DFIG wind turbine model with validation. The modeling includes the wind turbine aerodynamic rotor and

drive train representations which are often oversimplified. The wind turbine and wind farm models presented can be used for educational activities in wind power integration studies. Furthermore, they can be used to perform many real-world studies, such as power curve generation, wind power integration, short-circuit, dynamic interactions between wind turbines, power system dynamic stability and so on.

# Appendix

## Machine Specifications

| | |
|---|---|
| Poles | 6 |
| Rated voltage (l–l) | 690 V |
| Rated power | 1.8 MVA |
| Base angular frequency | 376.99 rad/s |
| Stator/rotor turns ratio | 0.379 |
| Angular moment of inertia | 0.578 s |
| Stator rotor resistance | 0.0054 p.u. |
| Wound rotor resistance | $10^{-6}$ p.u. |
| Magnetizing inductance | 6.83309 p.u. |
| Stator leakage inductance | 0.08 p.u. |
| Rotor leakage inductance | 0.04782 p.u. |

## Mechanical Data for Shaft Model

| | |
|---|---|
| $J_{rot}$ Rotor moment of inertia (kg mm) | $J_{rot} = 4{,}950{,}000$ kg mm |
| $J_{gen}$ Generator moment of inertia (kg mm) | $J_{gen} = 80$ |
| $J_{q2}$ Gearbox moment of inertia (kg mm) | $J_{q2} = 15$ kg mm |
| $K_{rq1}$ Spring constant rotor shaft (Nm/rad) | $K_{rq1} = 9{,}800{,}000$ Nm/rad |
| $K_{q2g}$ Spring constant generator shaft (Nm/rad) | $K_{q2g} = 2{,}950{,}000$ Nm/rad |
| $D_{rot}$ Damping rotor (Nms/rad) | $D_{rot} = 0$ Nms/rad |
| $D_{rot}$ Damping gearbox (Nms/rad) | $D_{q2} = 2.4$ Nms/rad |
| $D_{rot}$ Damping generator (Nms/rad) | $D_{gen} = 0$ Nms/rad |
| $D_{rot}$ Damping rotor shaft (Nms/rad) | $D_{rq1} = 13{,}500$ Nms/rad |
| $D_{rot}$ Damping generator shaft (Nms/rad) | $D_{q2g} = 30$ Nms/rad |
| $f_n$ Nominal frequency (Hz) | $f_n = 60$ Hz |
| $P_{gn}$ Nominal mechanical power (MW) | $P_{gn} = 1.5$ MW |
| $a$ Gear ratio | $a = 70$ |
| $p$ Generator pole pairs | $p = 3$ |

## Nomenclature

| | |
|---|---|
| $\lambda_r$ | Tip speed ratio |
| $\rho$ | Air density |
| $\lambda$ | Flux linkage |
| $f$ | Frequency |
| $P$ | Real power |
| $Q$ | Reactive power |
| $V$ | Voltage |
| $I$ | Current |
| $L$ | Inductance |
| $R$ | Resistance |
| $\beta$ | Pitch angle of blades |
| $\beta_0$ | Initial Pitch angle of blades |
| $\beta_q$ | Angle measured from the positive stationary a-phase axis to the rotating q-axis |
| $\omega$ | Angular velocity |
| $\tau$ | Torque |
| $J$ | Moment of Inertia |
| $B$ | Damping constant |
| $K$ | Shaft stiffness |
| $N$ | Gear ratio |
| $\theta$ | Twist in shaft |

## Superscripts and Subscripts

| | |
|---|---|
| $'$ | Parameter referred to stator |
| $s$ | Stator quantity |
| $r$ | Rotor quantity |
| $d$ | $d$-axis quantity |
| $q$ | $q$-axis quantity |
| $abc$ | Parameter in $abc$ reference frame |
| $qd0$ | Parameter in $qd0$ reference frame |
| $l$ | Leakage quantity (used with inductance) |
| $m$ | Mutual quantity (used with inductance) |
| $rms$ | Root mean square quantity |
| $ph$ | Phase quantity |
| $1\phi$ | Single-phase quantity |
| $3\phi$ | Three-phase quantity |
| $G$, $gen$ | Generator |
| $T$, $rot$ | Rotor |
| $eqv$ | Equivalent value (generator and rotor combined) |

## References


1. 20 % Wind Energy by 2030: Increasing Wind Energy's Contribution to U.S. Electricity Supply, U.S. D.O.E., July 2008
2. Ackermann T (ed) (2005) Wind power in power systems. Wiley, New York
3. Hansen AD, Hansen LH (2007) Wind turbine concept market penetration over 10 years (1995–2004). Wind Energy 10(1):81–97 (Wiley Online Library)
4. Slootweg JG, Polinder H, Kling WL (2001) *D*ynamic modeling of a wind turbine with doubly fed induction generator. In: Proceedings of 2001 power engineering society summer meeting, 2001. IEEE, vol 1. pp. 644–649
5. Uctug MY, Eskandarzadeh I, Ince H (1994). Modeling and output power optimization of a wind turbine driven double output induction generator. Electric power applications, IEE proceedings, vol 141. pp 33–38
6. Kim S-K, Kim E-S, Yoon J-Y, Kim H-Y (2004) PSCAD/EMTDC based dynamic modeling and analysis of a variable speed wind turbine. In: Proceedings of 2004 power engineering society general meeting, 2004. IEEE, vol 2. pp 1735–1741
7. Slootweg JG, Kling WL (2003) Aggregated modeling of wind parks in power system dynamics simulations. In: Proceedings of 2003 power tech conference proceedings, 2003 IEEE Bologna, vol 3. p 6
8. Delaleau E, Stankovic AM, Dynamic phasor modeling of the doubly-fed induction machine in generator operation. www.ece.northeastern.edu/faculty/stankovic/Conf_papers/lsiwp03.pdf
9. Gagnon R, Sybille G, Bernard S, Pare D, Casoria S, Larose C (2005) Modeling and real-time simulation of a doubly-fed induction generator driven by a wind turbine. www.ipst.org/TechPapers/2005/IPST05_Paper162.pdf
10. Lubosny Z (2003) Wind turbine operation in electric power systems: advanced modeling. Springer, Berlin
11. Akhmatov V (2005) Induction generators for wind power. Multiscience Publishing Company, Essex, UK
12. Manwell JF, McGowan JG, Rogers AL (2003) Wind energy explained: theory design and applications. Wiley, New York England Reprinted with corrections August
13. Krause PC (1986) Analysis of electric machinery. McGraw Hill Co, New York
14. Burnham DJ, Santoso S, Muljadi E (2009) Variable rotor resistance control of wind turbine generators. In: Power and energy society general meeting, 2009. PES' 09. IEEE, 26–30 July 2009
15. Hang CC, Astrom KJ, Ho WK (1991) Refinements of the Ziegler-Nichols tuning formula. Control Theory and Applications, IEE Proceedings D, vol 138, No. 2
16. E. Muljadi and C.P. Butterfield, Pitch-controlled variable-speed wind turbine generation. In: Industry applications conference, 1999. Thirty-fourth IAS annual meeting. conference record of the 1999 IEEE, vol 1. pp 323–330. 3–7 October 1999
17. Singh M, Santoso S (2007) Electromechanical and time-domain modeling of wind generators. Power engineering society general meeting, 2007. IEEE, 24–28 June 2007
18. Singh M, Faria K, Santoso S, Muljadi E (2009) Validation and analysis of wind power plant models using short-circuit field measurement data. Power & energy society general meeting, 2009. PES '09. IEEE, 26–30 July 2009
19. Santoso S, Hur K, Zhou Z (2006) Induction machine modeling for distribution system analysis—A time domain solution. Transmission and distribution conference and exhibition, 2005/2006 IEEE PES, pp 583–587. 21–24 May 2006
20. Muljadi E, Butterfield CP, Ellis A, Mechenbier J, Hochheimer J, Young R, Miller N, Delmerico R, Zavadil R, Smith JC (2006) Equivalencing the collector system of a large wind power plant. IEEE power engineering society, annual conference, Montreal, Quebec, 2006 IEEE PES

21. Muljadi E, Pasupulati S, Ellis A, Kosterov D (2008) Method of equivalencing for a large wind power plant with multiple turbine representation. In: 2008 IEEE power and energy society general meeting-conversion and delivery of electrical energy in the 21st century
22. Muljadi E, Ellis A (2008) Validation of wind power plant dynamic models. IEEE power engineering society general meeting, Pittsburgh, 20–24 July 2008
23. Muljadi E, Butterfield CP, Parsons B, Ellis A (2007) Effect of variable speed wind turbine generator on stability of a weak grid. IEEE Trans Energy Conversion 22(1):29–36
24. Muljadi E, Nguyen TB, Pai MA (2008) Impact of wind power plants on voltage and transient stability of power systems. In: Energy 2030 conference, 2008. ENERGY 2008. IEEE, 17–18 Nov 2008